Petroleum Science 22 (2025) 4624–4644

Contents lists available at ScienceDirect

Petroleum Science

journal homepage: www.keaipublishing.com/en/journals/petroleum-science

Original Paper

Risk-based design method for gas storage wellbore structure using grey geological information

Kai Wei [a,b], Zhe Xu [a,b,*], Ao Cai [a,b], Yan-Xian Wu [c], Yan Yan [d]

[a] State Key Laboratory of Low Carbon Catalysis and Carbon Dioxide Utilization (Yangtze University), Wuhan, 430100, Hubei, China
[b] National Engineering Research Center for Oil and Gas Drilling and Completion Technology (Yangtze University), Wuhan, 430100, Hubei, China
[c] Research Institute of Oil Production Technology, Xinjiang Oilfield Company, Karamay, 834000, Xinjiang, China
[d] State Key Laboratory of Oil and Gas Equipment, CNPC Tubular Goods Research Institute, Xi'an, 710077, Shaanxi, China

ARTICLE INFO

Article history:
Received 8 January 2025
Received in revised form
27 August 2025
Accepted 28 August 2025
Available online 2 September 2025

Edited by Jia-Jia Fei

Keywords:
Gas storage
Wellbore structure
Three parameter interval grey number
Safe drilling fluid density window
Risk design

ABSTRACT

Underground gas storage facilities play a crucial strategic role in ensuring the balance of natural gas supply and demand, addressing seasonal fluctuations, and responding to emergencies. The design of the wellbore structure is key to both construction and operation, directly influencing long-term efficiency and economic benefits. However, since gas storage is typically located in complex geological environments, parameters such as formation pressure, porosity, and fracture pressure exhibit significant spatial variation and uncertainty. Traditional design methods based on deterministic geological data struggle to accurately predict the drilling fluid density window, reducing design precision and reliability. To address this, this paper proposes an optimized design method based on grey geological information and a three-parameter drilling fluid density window. By constructing a model of the three-parameter density window, including upper and lower limits and the centroid, and developing drilling risk evaluation models for overflow, collapse, wellbore loss, and stuck pipe, the method combines procedural approaches with geometric plotting to determine casing levels and depth. Case studies show that this method significantly improves the safety and economy of gas storage wellbore structure design, providing scientific guidance for similar complex gas storage well designs. The drilling risk evaluation model based on three-parameter grey intervals aligns closely with actual risks, validating its reliability and applicability. In practical engineering, a balanced wellbore structure design effectively ensures safety while controlling construction costs. This method offers flexible and reliable references for gas storage well design at different risk levels, holding significant practical value.

1. Introduction

Gas storage facilities, as important infrastructures for peak shaving, emergency reserves, and supply security of natural gas (Zhang et al., 2017), play a critical role in ensuring energy supply reliability and stability. With the rapid development of the economy and industrialization, the demand for natural gas is continuously increasing (Liu et al., 2018). In response to the growing natural gas demand, the construction of gas storage facilities has become a key measure in energy management and an essential component of ensuring the stability of energy supply. Through the effective construction and optimization of gas storage, seasonal fluctuations in natural gas supply can be alleviated, ensuring stable supply during the winter peak demand period, thus providing strong support for the smooth operation of the economy.

The wellbore structure design of gas storage facilities is a core component of the entire gas storage project. Compared with conventional well designs, it has significantly different technical requirements and economic considerations. Conventional well designs are typically based on relatively stable geological conditions and low-pressure operating conditions, while the design of gas storage wellbore structures must account for more complex geological conditions and high-pressure injection and production operations. Particularly under high throughput conditions, the wellbore structure of gas storage facilities must withstand frequent pressure fluctuations and challenges posed by reservoir heterogeneity, which significantly increases the design difficulty. The design specifications for the wellbore structure of gas storage

* Corresponding author.
E-mail address: xuzhe040733@163.com (Z. Xu).
Peer review under the responsibility of China University of Petroleum (Beijing).

https://doi.org/10.1016/j.petsci.2025.08.033

Nomenclature

d_j	The spatial distance from a point (H_j, N_j, E_j) on a neighboring well to a point (H_o, N_o, E_o) on the target well, m.
D ($\otimes$)	Depth grey number, m
$f(p_p)$, $f(p_c)$, $f(p_f)$, $f(p_j)$	The probability density functions of pore pressure, collapse pressure, fracture pressure, and stuck drilling pressure
$\rho(\otimes)$	Drilling fluid density grey number, g/cm^3
$q(\otimes)$	Three-parameter interval grey number
H_A^{sl}, H_A^{su}, H_O^{su}, H_O^{sl}	The upper and lower boundaries of wells WO and WA in the S formation
(H_j, N_j, E_j)	The coordinates of points corresponding to the well
H_j^s, P_j^s	The depth vector and formation parameter vector of formation S in neighboring well j, after depth adjustment and inverse distance weighting interpolation, respectively
H_{j0}, H_{j1}	The lower and upper bounds of the grey-number band for the upper limit of drilling fluid density, respectively
L_{j0}, L_{j1}	The lower and upper bounds of the grey-number band for the lower limit of drilling fluid density, respectively
L_{j^*}, H_{j^*}	The maximum probable values based on grey information
M_{bo}	Grey safety drilling fluid density window
p_{c0}, p_{c1}, p_{c2}	The lower limit, upper limit, and centroid of formation collapse pressure, respectively
p_d	Drilling fluid density, g/cm^3
p_{f0}, p_{f1}, p_{f2}	The lower limit, upper limit, and centroid of formation fracture pressure, respectively
p_{j0}, p_{j1}, p_{j2}	The lower limit, upper limit, and centroid of formation stuck drilling pressure, respectively
p_{p0}, p_{p1}, p_{p2}	The lower limit, upper limit, and centroid of formation pore pressure, respectively
$\underline{q}$, $\tilde{q}$, $\overline{q}$	The lower limit, centroid, and upper limit of geological parameters
S	Formation
S_{risk}	Risk domain area
$\underline{w}$, $\tilde{w}$, $\overline{w}$	The probabilities corresponding to the lower limit, the center of gravity, and the upper limit
λ	Weighted power index
H, Pl, Pu	Programmatically designed array

facilities differ from those of conventional wells, generally requiring higher strength and stability to ensure safety and reliability during long-term operation under high-pressure, high-flow injection and production conditions. As a result, the wellbore structure design (Guan et al., 2001) of gas storage facilities requires more detailed parameter analysis and optimization, which also leads to relatively higher construction costs.

Therefore, in response to these issues, expert teams from around the world have proposed a series of innovative design methods for gas storage facilities, achieving significant results in the design and construction technologies of gas storage systems. Iwaszczuk et al. (2022) considered the underground gas storage system, its development history, the characteristics of regional gas storage complexes, and the current situation and role of natural gas companies in the natural gas market, thereby demonstrating the important role of underground gas storage in ensuring Europe's energy supply. Zhang et al. (2020) investigated the current status and development direction of the natural gas market (NGM) in China, analyzing in detail regional differences, seasonal variations, and the impact of imports, and clarified the peak-shaving demand for natural gas supply nationwide. Du et al. (2024) studied the feasibility of using CO_2 as a buffer gas in underground natural gas storage and its impact on the properties of mixed gases. This study provides an important theoretical basis for the application of CO_2 in underground gas storage, indicating that using CO_2 as a buffer gas can improve the comprehensive performance of gas storage facilities. Kowalski et al. (2023) used compositional numerical simulations to investigate how different permeability and pore structures affect the performance of underground gas storage with CO_2 as a buffer gas. This research provides a theoretical basis for enhancing the peak-shaving capacity of gas storage and optimizing reservoir design, helping to improve the overall performance and operational efficiency of gas storage construction. Mu et al. (2019) explored the use of CO_2 as a cushion gas in underground gas storage (UGS), emphasizing its importance in maintaining reservoir pressure and ensuring UGS stability. Through numerical simulation, they analyzed the dissolution effects of CO_2 and water, as well as the diffusion between gases, modeling the injection and production processes of UGS with CO_2 as a buffer gas. This study provides a scientific basis for optimizing the operational efficiency of gas storage and understanding its dynamic behavior. Lin et al. (2023) studied the simulation and optimization of surface gas injection systems for practical underground gas storage. Based on the ideal gas law, Van der Waals equation, and the Redlich–Kwong equation, they proposed calculation formulas for injection well pressures, which were verified with actual data. Molíková et al. (2022) focused on revealing microbial activity in underground gas reservoirs, optimizing methane generation conditions, and developing biomethanation technology to promote the low-carbon, environmentally friendly application of underground gas storage and greenhouse gas reduction. Jiang et al. (2021) developed integrated oil recovery and underground gas storage technologies to optimize gas storage construction and operation, successfully improving oil recovery and the economic benefits of gas storage, and established a safety monitoring and early warning system for gas storage facilities, enhancing their safety. Their work also advanced geological modeling and numerical simulation technologies for gas storage, providing strong technical support for the long-term stable operation and sustainable development of gas storage facilities. Sadeghi and Sedaee (2022) successfully reduced the base gas cost of underground natural gas storage by introducing nitrogen and carbon dioxide as alternative buffer gases, and studied the gas mixing effects through numerical simulations, optimizing the operating conditions of gas storage, improving gas recovery heating values, and enhancing the safety and economic

efficiency of gas storage. Yu et al. (2019) developed an integrated approach to assess the supply reliability of natural gas pipeline systems, focusing on the hydraulic characteristics of underground gas storage and the uncertainties in injection/production capacities. The method ensures stable gas supply during demand-supply imbalances by adjusting the injection and production functions of gas storage. Monte Carlo simulations validated the feasibility of the approach, highlighting that ignoring the uncertainty of gas storage capacity could lead to an overestimation of supply reliability. Zheng et al. (2017) proposed key evaluation technologies for gas reservoir conversion to underground gas storage, analyzing field applications and summarizing the construction and operation experiences of China's first commercial underground gas storage facilities (UGS). They studied the high-throughput multi-cycle injection and production mechanisms in the short term, and developed four key technologies for UGS, including sealing evaluation, gas storage parameter design, well network optimization, and monitoring scheme design. Tang et al. (2016) experimentally studied gas-gas and gas-water alternating seepage, establishing an improved inflow-performance equation that accounts for water invasion effects. The equation was validated through case studies, and the results indicated that permeability changes during the conversion of a reservoir to underground gas storage. The modified equation accurately predicted the inflow performance of gas storage. Sedaee et al. (2019) developed an integrated modeling approach for the underground gas storage process in salt caverns, covering key elements such as salt dissolution, gas injection, production, heat transfer, and hydrate formation. By numerically solving the model equations, they developed the first software with specified functions, "UT-SCUGS". Xue et al. (2023) developed an integrated model for the complexity of underground gas storage in depleted oil and gas reservoir fractured structures, coupling wellbore, reservoir, and natural gas properties for the first time to address the lack of numerical models in gas storage construction. The model significantly improved calculation efficiency and ensured global mass conservation during long-term operations by proposing new gas flow direction factors, hydrocarbon source terms, and pressure correction methods.

However, the wellbore structure design of gas storage facilities still faces a series of challenges, including complex geological conditions and incomplete geological information (Hund, 1986). The design of gas storage wellbore structures involves multiple factors, including geological conditions, wellbore structure parameters, and construction techniques. Existing design methods primarily rely on deterministic geological information, typically analyzing wellbore structure design parameters directly from geological survey data. Geological survey data includes key parameters such as formation pressure, pore pressure, collapse pressure, and fracture pressure, which play a critical role in the design process. However, due to the complexity and uncertainty of geological conditions, these data often exhibit measurement errors in practice, which can affect the precision and reliability of the design. For example, in traditional geological exploration methods, the mechanical parameters and pressures of underground rock formations are estimated by placing explosive charges in boreholes on the surface and measuring the difference between incident and reflected seismic waves. However, the interpretation and decoding of seismic data are complex and prone to errors, leading to unavoidable uncertainty in the geological parameters. This uncertainty not only increases the difficulty of design but may also pose unexpected safety hazards during construction.

In the case of limited geological information, existing design methods often fail to fully account for the uncertainty and vagueness inherent in geological data. The limitations of geological exploration and measurement technologies (Xu et al., 2022) result in a broad range of grey areas in the geological data. To ensure the safe operation of gas storage facilities, there is an urgent need for more scientific and accurate design methods. In recent years, an increasing number of researchers have started exploring design methods based on uncertainty information. Among them, grey system theory, proposed by professor Deng Ju-long, is an effective method for dealing with incomplete information and uncertainty, and has been widely applied in engineering design and risk analysis (Xu et al., 2023). In addition, Wei et al. (2013) established a monitoring and evaluation method for drilling engineering risks based on BP neural networks and Monte Carlo stochastic simulation, targeting the correlation between drilling engineering monitoring parameters and downhole complex accidents, as well as their inherent uncertainties. This method provides an effective means for risk identification and decision-making under complex conditions. Sheng et al. (2021) constructed a distribution model to dynamically correct formation pressure by integrating LWD real-time data with probability statistics theory, and established a risk quantitative assessment framework by combining pressure balance constraint equations. This study will further extend the application of grey information theory in gas storage design. By introducing the centroid parameter, it can more accurately characterize uncertainties in geological information. Through the three-parameter safety drilling fluid density window, it is possible to scientifically assess design risks and optimize wellbore structure design under complex geological conditions.

The introduction of the three-parameter safety drilling fluid density window represents a significant improvement over the traditional two-parameter method. Traditional safety drilling fluid density windows (Zhang et al., 2019) typically include only two parameters: the upper and lower limits, which are insufficient to fully capture the uncertainty in geological information. In contrast, the three-parameter method incorporates a centroid parameter, enabling designers to more accurately describe and control the uncertainty of subsurface geological conditions. The application of the three-parameter safety drilling fluid density window in gas storage wellbore structure design allows for a better assurance of both the rationality and economic feasibility of the design.

Specifically, the application of the three-parameter safety drilling fluid density window in gas storage wellbore structure design not only enhances the precision of the design but also significantly reduces the risks during construction. By more accurately describing the uncertainties in geological information, designers can better predict potential geological issues and formulate corresponding preventive measures. The use of this method effectively addresses the complexity and uncertainty of geological conditions, significantly improving the economic feasibility of the gas storage facility and providing technical support for the successful implementation of related projects.

Furthermore, in the practical application of gas storage wellbore structure design, the combination of grey information theory with the three-parameter safety drilling fluid density window can significantly improve the scientific and reliable nature of the design. Specific case studies show that this method achieves favorable results in complex geological environments. For example, in a real gas storage project, by inputting actual geological data into the model, designers were able to more accurately assess the risks associated with geological conditions and optimize the design, thereby improving the safety and economic efficiency of the gas storage wellbore structure. These successful cases further validate the effectiveness and reliability of the method, providing valuable experience and insights for future gas storage construction.

In summary, optimizing gas storage wellbore structure design, particularly by incorporating grey information theory under complex geological conditions, significantly enhances the

scientific and rational aspects of the design and reduces risks. The application of this method not only helps improve the safety and economic feasibility of gas storage but also provides solid technical support for the implementation of national energy security strategies. As the demand for gas storage construction continues to grow, design methods based on grey information theory and the three-parameter safety drilling fluid density window will find broader applications, offering more reliable technical support for the energy security of our country.

2. Methodology

2.1. Three-parameter safe drilling fluid density window

Grey information has become an effective tool for addressing geological uncertainties due to its unique advantages under incomplete information conditions. In contrast to traditional probabilistic statistical methods that rely on large sample data, grey information theory employs its distinctive modeling mechanisms to establish stable prediction models under small-sample conditions, significantly reducing reliance on large data volumes. In this paper, the centroid parameter in grey information theory will be used to describe the uncertainty of geological information, thereby determining the construction of a safe drilling fluid density window. The core of this modeling mechanism lies in the introduction of "grey numbers", which are a type of fuzzy number with known possible value ranges but unknown specific values, typically denoted by the symbol $\otimes$. An interval grey number refers to a grey number with a clear upper limit $\overline{a}$ and lower limit $\underline{a}$, denoted as $a(\otimes) \in (\underline{a}, \overline{a})$. A three-parameter interval grey number, on the other hand, not only has upper and lower bounds but also a centroid $\tilde{a}$, representing the most likely value within the range, and is denoted as $a(\otimes) \in (\underline{a}, \tilde{a}, \overline{a})$. Supposing a certain geological parameter is a three-parameter interval grey number $q(\circledast)$ (Li and Zhu, 2019), if its value range and the number with the highest possibility of taking a value are known, then this geological parameter can be expressed as shown in Eq. (1).

$$\begin{cases} q(\otimes) \in \left[\underline{q}(\underline{w}), \tilde{q}(\tilde{w}), \overline{q}(\overline{w})\right]\left(\underline{q} \le \tilde{q} \le \overline{q}\right) \\ \int_{\underline{q}}^{\tilde{q}} f(q) = 1 \end{cases} \tag{1}$$

In the formula, $\underline{q}$ and $\overline{q}$ respectively represent the lower limit and upper limit of the value of the geological parameter, $\tilde{q}$ is called the center of gravity, and $q(\circledast)$ represents the value with the greatest possibility of taking the value of the geological parameter; $\underline{w}$, $\tilde{w}$, and $\overline{w}$ respectively represent the probabilities corresponding to the lower limit, the center of gravity, and the upper limit, and are also called the degrees of credibility.

Three-parameter grey numbers can also undergo basic arithmetic operations. Supposing there are two three-parameter interval grey numbers, $a(\otimes) \in [\underline{a}(\underline{w}^a), \tilde{a}(\tilde{w}^a), \overline{a}(\underline{w}^a)](\underline{a} \le \tilde{a} \le \overline{a})$ and $b(\otimes) \in \left[\underline{b}\left(\underline{w}^b\right), \tilde{b}(\tilde{w}^b), \overline{b}(\overline{w}^b)\right](\underline{b} \le \tilde{b} \le \overline{b})$, the operational rules are shown in Eq. (2).

$$\begin{cases} ka(\otimes) \in [k\underline{a}, k\tilde{a}, k\overline{a}](k \ge 0) \\ ka(\otimes) \in [k\overline{a}, k\tilde{a}, k\underline{a}](k \le 0) \\ a(\otimes)^n \in [\underline{a}^n, \tilde{a}^n, \overline{a}^n](n \ge 0) \\ k^{a(\otimes)} \in \left[k^{\underline{a}}, k^{\tilde{a}}, k^{\overline{a}}\right](k > 0) \\ a(\otimes) \pm b(\otimes) \in \left[(\underline{a}\cdot\underline{w}^a) \pm \left(\underline{b}\cdot\underline{w}^b\right), (\tilde{a}\cdot\tilde{w}^a) \pm \left(\tilde{b}\cdot\tilde{w}^b\right), (\overline{a}\cdot\overline{w}^a) \pm \left(\overline{b}\cdot\overline{w}^b\right)\right] \\ a(\otimes) \times b(\otimes) \in \begin{bmatrix} \min\left((\underline{a}\cdot\underline{w}^a)\cdot\left(\underline{b}\cdot\underline{w}^b\right), (\underline{a}\cdot\underline{w}^a)\cdot\left(\overline{b}\cdot\overline{w}^b\right), (\overline{a}\cdot\overline{w}^a)\cdot\left(\underline{b}\cdot\underline{w}^b\right), (\overline{a}\cdot\overline{w}^a)\cdot\left(\overline{b}\cdot\overline{w}^b\right)\right), \\ (\tilde{a}\cdot\tilde{w}^a)\cdot\left(\tilde{b}\cdot\tilde{w}^b\right), \\ \max\left((\underline{a}\cdot\underline{w}^a)\cdot\left(\underline{b}\cdot\underline{w}^b\right), (\underline{a}\cdot\underline{w}^a)\cdot\left(\overline{b}\cdot\overline{w}^b\right), (\overline{a}\cdot\overline{w}^a)\cdot\left(\underline{b}\cdot\underline{w}^b\right), (\overline{a}\cdot\overline{w}^a)\cdot\left(\overline{b}\cdot\overline{w}^b\right)\right) \end{bmatrix} \\ a(\otimes)/b(\otimes) \in \begin{bmatrix} \min\left((\underline{a}\cdot\underline{w}^a)\Big/\left(\underline{b}\cdot\underline{w}^b\right), (\underline{a}\cdot\underline{w}^a)\Big/\left(\overline{b}\cdot\overline{w}^b\right), (\overline{a}\cdot\overline{w}^a)\Big/\left(\underline{b}\cdot\underline{w}^b\right), (\overline{a}\cdot\overline{w}^a)\Big/\left(\overline{b}\cdot\overline{w}^b\right)\right), \\ (\tilde{a}\cdot\tilde{w}^a)\cdot\left(\tilde{b}\cdot\tilde{w}^b\right), \\ \max\left((\underline{a}\cdot\underline{w}^a)\Big/\left(\underline{b}\cdot\underline{w}^b\right), (\underline{a}\cdot\underline{w}^a)\Big/\left(\overline{b}\cdot\overline{w}^b\right), (\overline{a}\cdot\overline{w}^a)\Big/\left(\underline{b}\cdot\underline{w}^b\right), (\overline{a}\cdot\overline{w}^a)\Big/\left(\overline{b}\cdot\overline{w}^b\right)\right) \end{bmatrix} \end{cases} \tag{2}$$

The safe drilling fluid density window is a key factor affecting drilling safety. However, due to the complexity and uncertainty of objective geological conditions and the limitations of technical level and other factors, when using the data of drilled adjacent wells to predict (Diaz and Kim, 2020) the safe drilling fluid density window of the target well in the same area, relatively large uncertainties will arise and it has grey attributes, which can be called a grey safe drilling fluid density window. In order to facilitate scientific characterization and calculation, the well depth, parameter lower limit, parameter center of gravity, and parameter

upper limit can be set in the form of a matrix (Wei et al., 2020) as shown in Eq. (3).

$$\boldsymbol{M}_{\mathrm{b}} = [\boldsymbol{H}, \boldsymbol{P}] = \left[\boldsymbol{H}, \underline{\boldsymbol{p}}, \tilde{\boldsymbol{p}}, \overline{\boldsymbol{p}}\right] \tag{3}$$

In the formula, $\boldsymbol{M}_{\mathrm{b}}$ is the wellbore matrix which is composed of two parts: depth and parameter; $\boldsymbol{H}$ represents a one-dimensional depth column array; $\boldsymbol{P}$ represents a one-dimensional parameter matrix. For the three-parameter interval grey number (Li et al., 2016), it is composed of three parts: the lower limit column array $\underline{\boldsymbol{p}}$, the center of gravity column array $\tilde{\boldsymbol{p}}$, and the upper limit column array $\overline{\boldsymbol{p}}$.

Due to the influence of the undulation, thickness variation, extension trend of the strata and the faults, when using the information of adjacent wells in the region to construct the safe drilling fluid density, it is necessary to fully consider the spatial distribution of the strata and the distance between wells (He et al., 2012). Therefore, when constructing the grey safe drilling fluid density window of the target well, the depth column array and the parameter matrix of the three-parameter interval grey number wellbore matrix of adjacent wells are respectively subjected to depth adjustment and inverse distance weighting interpolation processing (Zhang et al., 2024).

According to the stratum comparison in engineering practice, it can be known that due to the influence of the undulation, thickness variation, extension trend and faults of the strata, the burial depth and thickness of the strata of the target well (WO) and adjacent wells (WA, WB, WC, WD) are not necessarily equal, as shown in Fig. 1. Therefore, when transplanting the stratum information of adjacent wells to the target well, it is first necessary to carry out the adjustment processing on the well depth part of the wellbore matrix of the adjacent wells in the target stratum (Wei et al., 2024).

Taking Fig. 1 as an example, when transplanting the S stratum information of the adjacent well WA to the target well WO, it is first necessary to align the upper bound H_A^{Su} and the lower bound H_A^{Sl} of WA with the upper bound H_O^{Su} and the lower bound H_O^{Sl} of the S stratum of the target well in the direction indicated by the arrow in the figure. Therefore, the wellbore depth matrix of the jth adjacent well (Hong et al., 2020) becomes as shown in Eq. (4) after depth adjustment processing.

$$\boldsymbol{H}_j^S = \begin{bmatrix} \left(H_{\mathrm{O}}^{\mathrm{su}} - \dfrac{H_j^{\mathrm{su}}\left(H_{\mathrm{O}}^{\mathrm{sl}} - H_{\mathrm{O}}^{\mathrm{su}}\right)}{H_j^{\mathrm{sl}} - H_j^{\mathrm{su}}}\right) \begin{bmatrix} 1 \\ \vdots \\ 1 \\ \vdots \\ 1 \end{bmatrix} + \dfrac{H_{\mathrm{O}}^{\mathrm{sl}} - H_{\mathrm{O}}^{\mathrm{su}}}{H_j^{\mathrm{sl}} - H_j^{\mathrm{su}}} \begin{bmatrix} h_j^{k\mathrm{u}} \\ \vdots \\ h_j^{kn} \\ \vdots \\ h_j^{k\mathrm{l}} \end{bmatrix} \end{bmatrix} \tag{4}$$

In the equation, $\boldsymbol{H}_j^S$ represents the depth column vector of stratum S of adjacent well j after depth adjustment processing; $H_{\mathrm{O}}^{\mathrm{su}}$ and $H_{\mathrm{O}}^{\mathrm{sl}}$ respectively represent the upper bound depth and the lower bound depth of stratum S of the target well WO; H_j^{su} and H_j^{sl} respectively represent the upper bound depth and the lower bound depth of stratum S of adjacent well j; h_j^{km} represents the well depth at a certain depth of adjacent well j.

For the same block, assuming continuity within the rock layers and that the same rock layer is a transversely isotropic body, the influence of neighboring wells on the formation parameters of the target well varies due to differences in distances between the neighboring wells and the target well. It is generally considered that the closer a neighboring well is to the target well, the greater its influence on the formation information of the target well, while the farther a neighboring well is, the smaller its influence, which may even be negligible. Therefore, distance can be used as a weighting factor to correct the formation parameter matrix of the wellbore.

Supposing there are N drilled adjacent wells, and the formation pressure matrices of each interval have been established, the coordinates of the target point of the target well are (N_{O}, E_{O}, H_{O}), and the coordinates of the corresponding points on the adjacent wells with similar geological parameters to this point are (N_j, E_j, H_j), $j = 1, 2, \ldots, N$. The spatial distance relationships among each point are shown in Fig. 2.

For directional wells, the wellbore trajectory parameters (Hoseinpour and Riahi, 2022) influence the distance between the corresponding points of the adjacent wells and the target well. Based on the inverse distance weighting interpolation method, the

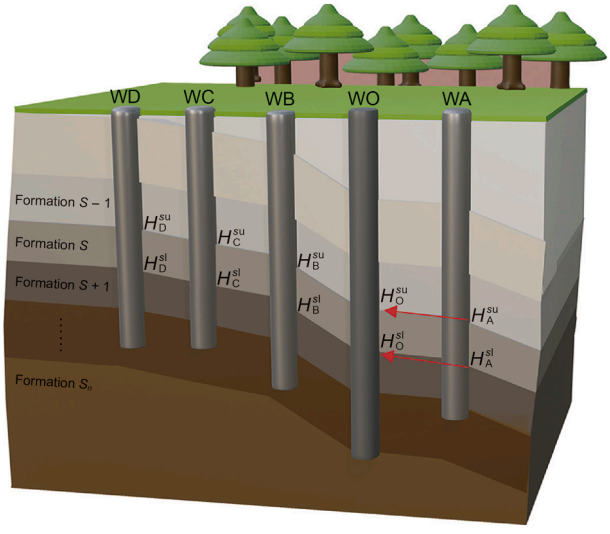

Fig. 1. Schematic diagram of stratigraphic correlation between different wells.

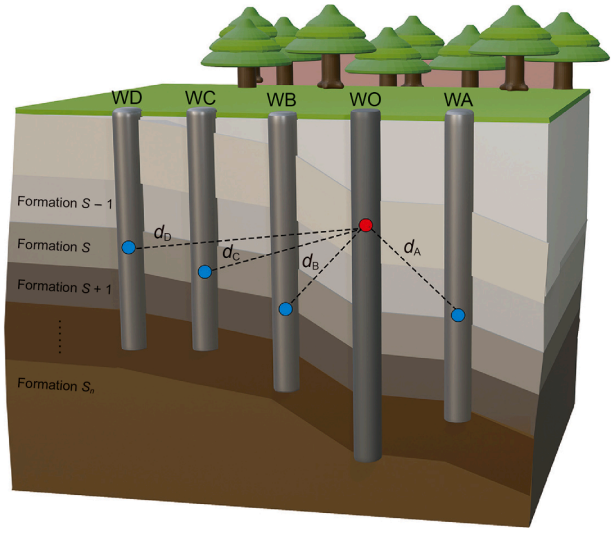

Fig. 2. Schematic diagram of spatial distance between points with similar geological parameters.

parameter column vector of the jth well in formation S of the target well is expressed as Eq. (5).

$$\begin{cases} \boldsymbol{P}_j^s = \dfrac{\dfrac{1}{d_j^\lambda}}{\sum\limits_j^{\mathrm{N}} \dfrac{1}{d_j^\lambda}} \begin{bmatrix} p_j^{\mathrm{ku}} & \cdots & p_j^{kn} & \cdots & p_j^{\mathrm{kl}} \end{bmatrix}^T \\ d_j = \sqrt{\left(H_{\mathrm{O}} - H_j\right)^2 + \left(N_{\mathrm{O}} - N_j\right)^2 + \left(E_{\mathrm{O}} - E_j\right)^2} \end{cases}, j = 1, 2, \cdots, N \tag{5}$$

In the equation, $\boldsymbol{P}_j^s$ represents the formation parameter column vector of formation S in neighboring well j after inverse distance weighting interpolation; d_j represents the spatial distance from a point (H_j, N_j, E_j) on the adjacent well to a point $(H_{\mathrm{O}}, N_{\mathrm{O}}, E_{\mathrm{O}})$ on the target well; λ is a constant greater than 0, referred to as the weighting power exponent. The larger the weighting power exponent λ, the greater the influence of the information of adjacent wells on the target well; N is the number of adjacent wells.

The three parameters of grey numbers can be obtained through the statistical analysis of information from adjacent wells. The minimum value among these parameters serves as the lower limit of the grey numbers within the geological interval of the target well, as shown in Eq. (6).

$$\left(p_j^{kn}\right)_{\min} = \min\left(\frac{\frac{1}{d_1^\lambda}}{\sum\limits_j^{\mathrm{N}} \frac{1}{d_j^\lambda}} p_1^{kn}, \cdots, \frac{\frac{1}{d_j^\lambda}}{\sum\limits_j^{\mathrm{N}} \frac{1}{d_j^\lambda}} p_j^{kn}, \cdots, \frac{\frac{1}{d_N^\lambda}}{\sum\limits_j^{\mathrm{N}} \frac{1}{d_j^\lambda}} p_N^{kn} \right) \tag{6}$$

The maximum value among these parameters serves as the upper limit of the grey numbers within the geological interval of the target well, as shown in Eq. (7).

$$\left(p_j^{kn}\right)_{\max} = \max\left(\frac{\frac{1}{d_1^\lambda}}{\sum\limits_j^{\mathrm{N}} \frac{1}{d_j^\lambda}} p_1^{kn}, \cdots, \frac{\frac{1}{d_j^\lambda}}{\sum\limits_j^{\mathrm{N}} \frac{1}{d_j^\lambda}} p_j^{kn}, \cdots, \frac{\frac{1}{d_N^\lambda}}{\sum\limits_j^{\mathrm{N}} \frac{1}{d_j^\lambda}} p_N^{kn} \right) \tag{7}$$

The weighted sum serves as the centroid of the interval grey number, as shown in Eq. (8).

$$\left(p_j^{kn}\right)_w = \frac{\frac{1}{d_1^\lambda}}{\sum\limits_j^{\mathrm{N}} \frac{1}{d_j^\lambda}} p_1^{kn} + \cdots + \frac{\frac{1}{d_j^\lambda}}{\sum\limits_j^{\mathrm{N}} \frac{1}{d_j^\lambda}} p_j^{kn} + \cdots + \frac{\frac{1}{d_N^\lambda}}{\sum\limits_j^{\mathrm{N}} \frac{1}{d_j^\lambda}} p_N^{kn} \tag{8}$$

Based on the above calculation methods, the three parameters of interval grey number safe drilling fluid density window of the target well can be determined, as shown in Eq. (9).

$$\boldsymbol{M}_{\mathrm{bo}}^s = \left[\left[\left(H_{\mathrm{O}}^{\mathrm{su}} - \frac{H_j^{\mathrm{su}}\left(H_{\mathrm{O}}^{\mathrm{sl}} - H_{\mathrm{O}}^{\mathrm{su}}\right)}{H_j^{\mathrm{sl}} - H_j^{\mathrm{su}}} \right) \begin{bmatrix} 1 \\ \vdots \\ 1 \\ \vdots \\ 1 \end{bmatrix} + \frac{H_{\mathrm{O}}^{\mathrm{sl}} - H_{\mathrm{O}}^{\mathrm{su}}}{H_j^{\mathrm{sl}} - H_j^{\mathrm{su}}} \begin{bmatrix} h_j^{\mathrm{ku}} \\ \vdots \\ h_j^{kn} \\ \vdots \\ h_j^{\mathrm{kl}} \end{bmatrix} \right] \times \begin{bmatrix} \left(p_j^{\mathrm{ku}}\right)_{\min} & \left(p_j^{\mathrm{ku}}\right)_w & \left(p_j^{\mathrm{ku}}\right)_{\max} \\ \vdots & \vdots & \vdots \\ \left(p_j^{kn}\right)_{\min} & \left(p_j^{kn}\right)_w & \left(p_j^{kn}\right)_{\max} \\ \vdots & \vdots & \vdots \\ \left(p_j^{\mathrm{kl}}\right)_{\min} & \left(p_j^{\mathrm{kl}}\right)_w & \left(p_j^{\mathrm{kl}}\right)_{\max} \end{bmatrix} \right] \tag{9}$$

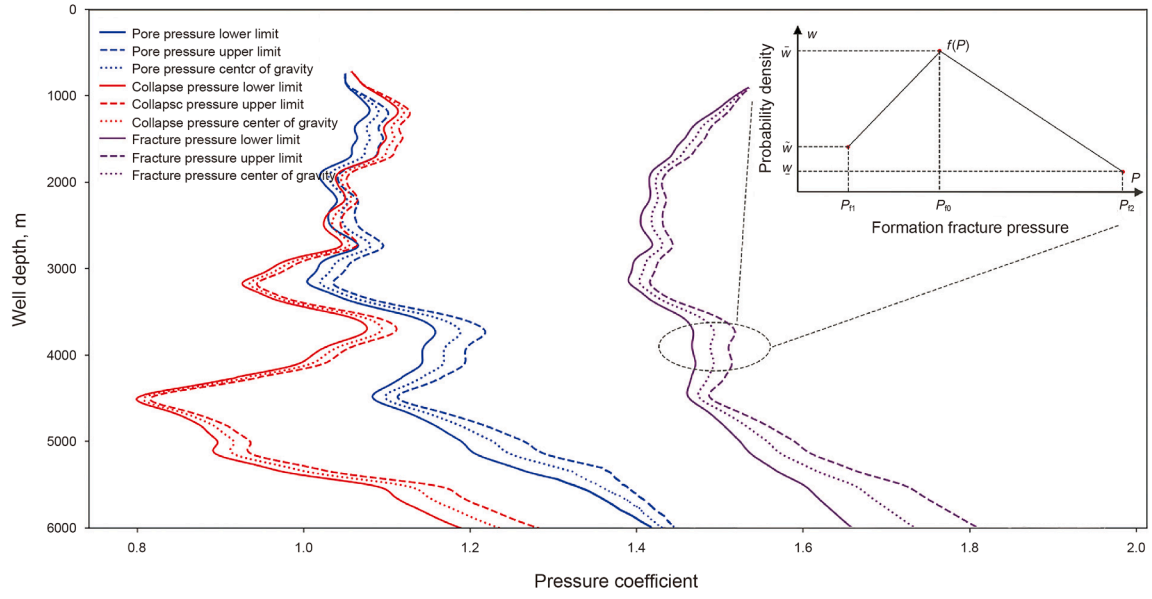

Fig. 3. Schematic diagram of formation pressure variation with depth.

By calculating the wellbore matrix layer by layer for the target well and assembling the individual matrices in the order of geological stratification, the complete wellbore information matrix for the target well can be obtained. This matrix represents the grey safe drilling fluid density window, as shown in Eq. (10).

$$\boldsymbol{M}_{\mathrm{bo}}=\begin{bmatrix}\vdots\\ \begin{bmatrix}\left(H_{\mathrm{O}}^{(s-1)\mathrm{u}}-\dfrac{H_j^{(s-1)\mathrm{u}}\left(H_{\mathrm{O}}^{(s-1)\mathrm{l}}-H_{\mathrm{O}}^{(s-1)\mathrm{u}}\right)}{H_j^{(s-1)\mathrm{l}}-H_j^{(s-1)\mathrm{u}}}\right)\begin{bmatrix}1\\ \vdots\\ 1\\ \vdots\\ 1\end{bmatrix}+\dfrac{H_{\mathrm{O}}^{(s-1)\mathrm{l}}-H_{\mathrm{O}}^{(s-1)\mathrm{u}}}{H_j^{(s-1)\mathrm{l}}-H_j^{(s-1)\mathrm{u}}}\begin{bmatrix}h_j^{k\mathrm{u}}\\ \vdots\\ h_j^{kn}\\ \vdots\\ h_j^{k\mathrm{l}}\end{bmatrix}\end{bmatrix}\begin{bmatrix}\left(p_j^{k\mathrm{u}}\right)_{\min} & \left(p_j^{k\mathrm{u}}\right)_w & \left(p_j^{k\mathrm{u}}\right)_{\max}\\ \vdots & \vdots & \vdots\\ \left(p_j^{kn}\right)_{\min} & \left(p_j^{kn}\right)_w & \left(p_j^{kn}\right)_{\max}\\ \vdots & \vdots & \vdots\\ \left(p_j^{k\mathrm{l}}\right)_{\min} & \left(p_j^{k\mathrm{l}}\right)_w & \left(p_j^{k\mathrm{l}}\right)_{\max}\end{bmatrix}\\ \begin{bmatrix}\left(H_{\mathrm{O}}^{\mathrm{su}}-\dfrac{H_j^{\mathrm{su}}\left(H_{\mathrm{O}}^{\mathrm{sl}}-H_{\mathrm{O}}^{\mathrm{su}}\right)}{H_j^{\mathrm{sl}}-H_j^{\mathrm{su}}}\right)\begin{bmatrix}1\\ \vdots\\ 1\\ \vdots\\ 1\end{bmatrix}+\dfrac{H_{\mathrm{O}}^{\mathrm{sl}}-H_{\mathrm{O}}^{\mathrm{su}}}{H_j^{\mathrm{sl}}-H_j^{\mathrm{su}}}\begin{bmatrix}h_j^{k\mathrm{u}}\\ \vdots\\ h_j^{kn}\\ \vdots\\ h_j^{k\mathrm{l}}\end{bmatrix}\end{bmatrix}\begin{bmatrix}\left(p_j^{k\mathrm{u}}\right)_{\min} & \left(p_j^{k\mathrm{u}}\right)_w & \left(p_j^{k\mathrm{u}}\right)_{\max}\\ \vdots & \vdots & \vdots\\ \left(p_j^{kn}\right)_{\min} & \left(p_j^{kn}\right)_w & \left(p_j^{kn}\right)_{\max}\\ \vdots & \vdots & \vdots\\ \left(p_j^{k\mathrm{l}}\right)_{\min} & \left(p_j^{k\mathrm{l}}\right)_w & \left(p_j^{k\mathrm{l}}\right)_{\max}\end{bmatrix}\\ \begin{bmatrix}\left(H_{\mathrm{O}}^{(s+1)\mathrm{u}}-\dfrac{H_j^{(s+1)\mathrm{u}}\left(H_{\mathrm{O}}^{(s+1)\mathrm{l}}-H_{\mathrm{O}}^{(s+1)\mathrm{u}}\right)}{H_j^{(s+1)\mathrm{l}}-H_j^{(s+1)\mathrm{u}}}\right)\begin{bmatrix}1\\ \vdots\\ 1\\ \vdots\\ 1\end{bmatrix}+\dfrac{H_{\mathrm{O}}^{(s+1)\mathrm{l}}-H_{\mathrm{O}}^{(s+1)\mathrm{u}}}{H_j^{(s+1)\mathrm{l}}-H_j^{(s+1)\mathrm{u}}}\begin{bmatrix}h_j^{k\mathrm{u}}\\ \vdots\\ h_j^{kn}\\ \vdots\\ h_j^{k\mathrm{l}}\end{bmatrix}\end{bmatrix}\begin{bmatrix}\left(p_j^{k\mathrm{u}}\right)_{\min} & \left(p_j^{k\mathrm{u}}\right)_w & \left(p_j^{k\mathrm{u}}\right)_{\max}\\ \vdots & \vdots & \vdots\\ \left(p_j^{kn}\right)_{\min} & \left(p_j^{kn}\right)_w & \left(p_j^{kn}\right)_{\max}\\ \vdots & \vdots & \vdots\\ \left(p_j^{k\mathrm{l}}\right)_{\min} & \left(p_j^{k\mathrm{l}}\right)_w & \left(p_j^{k\mathrm{l}}\right)_{\max}\end{bmatrix}\\ \vdots\end{bmatrix} \tag{10}$$

Based on geological exploration data and historical drilling records, key geological parameters such as pore pressure, collapse pressure, and fracture pressure were extracted. Using the three-parameter interval grey number method, a profile of formation pressure variation with depth was constructed, as shown in Fig. 3. The upper and lower bounds along with the centroid values of different pressure parameters collectively characterize the uncertainty of formation pressure. The embedded inset further illustrates the weight distribution of each parameter in the fracture pressure profile, quantifying the contribution ratios of the bounds and centroid to the pressure estimation.

2.2. Construction of risk evaluation model

Drilling is a concealed underground engineering operation. A mismatch between the density of the drilling fluid entering the wellbore and the safe drilling fluid density window of the formation is the fundamental cause of drilling risks such as overflow, lost circulation, wellbore collapse, and stuck pipe. Therefore, by analyzing the relationship between the drilling fluid density and the safe drilling fluid density window, the potential drilling risks can be assessed (Hu et al., 2022). Since the safe drilling fluid density window is composed of an upper safety limit and a lower safety limit, the corresponding drilling risks are discussed under two scenarios:

The first scenario involves drilling risks occurring when the drilling fluid density is lower than the lower limit of the safe drilling fluid density window, such as overflow and wellbore collapse. Taking the risk of overflow as an example, assume the formation pore pressure is represented by a three-parameter interval grey number that follows a probability density function $f(p_{\mathrm{p}})$, where the upper and lower limits denote the range of formation pore pressure values, and the centroid represents the most likely value of the formation pore pressure. p_{p1} represents the lower limit of the formation pore pressure, p_{p2} represents the upper limit, and p_{p0} represents the centroid (the most likely value). p_{d} denotes the actual value of the drilling fluid density.

As shown in Fig. 4, on the right side of the drilling fluid density line, where the drilling fluid density is less than the formation pore

pressure, formation fluids can easily invade the wellbore, resulting in an overflow risk. The integral area S_{risk} in this region quantifies the potential probability of overflow risk. On the left side of the drilling fluid density line, where the drilling fluid density exceeds the formation pore pressure, formation fluids are suppressed from entering the wellbore. The integral area S_{safe} in this region represents a safety domain associated with a lower probability of overflow occurrence.

In the figure, the vertical axis represents the probability density function $f(p_p)$. The closer the pressure value is to p_{p0}, the greater the corresponding w, indicating a higher probability of occurrence within the overall distribution. Therefore, the overflow risk probability calculation model is presented in Eq. (11).

For collapse risk, assume that the formation collapse pressure is represented as a three-parameter interval grey number that follows a probability density function $f(p_c)$, where the upper and lower limits indicate the range of formation collapse pressure values, and the centroid represents the most likely value of the formation collapse pressure. p_{c1} represents the lower limit of the formation collapse pressure, p_{c2} represents the upper limit, and p_{c0} represents the centroid (the most likely value). p_d denotes the actual value of the drilling fluid density. A schematic diagram for the calculation of collapse risk probability is shown in Fig. 5.

In the figure, the vertical axis represents the probability density function $f(p_c)$. The closer the pressure value is to p_{c0}, the greater the corresponding w, indicating a higher probability of occurrence

$$P = P\left(\rho_d < p_p\right) = \frac{S_{risk}}{S_{safe} + S_{risk}} = \frac{\int_{p_d}^{p_{p2}} f\left(p_p\right)\,dp_p}{\int_{p_{p1}}^{p_{p2}} f\left(p_p\right)\,dp_p}$$

$$= \begin{cases} 0 & \left(p_{p2} \le \rho_d\right) \\ \dfrac{\left[\dfrac{w_2 - w_1}{p_{p0} - p_{p2}}\left(\rho_d - p_{p0}\right) + w_2 + w_1\right]\left(p_{p2} - \rho_d\right)}{\left(w_1 + w_2\right)\left(p_{p2} - p_{p1}\right)} \times 100\% & \left(p_{p0} < \rho_d < p_{p2}\right) \\ \left\{\dfrac{p_{p2} - p_{p0}}{p_{p2} - p_{p1}} + \dfrac{\left[\dfrac{w_2 - w_1}{p_{p0} - p_{p1}}\left(\rho_d - p_{p0}\right) + w_2 + w_2\right]\left(p_{p0} - \rho_d\right)}{\left(w_1 + w_2\right)\left(p_{p2} - p_{p1}\right)}\right\} \times 100\% & \left(p_{p1} < \rho_d \le p_{p0}\right) \\ 100 & \left(\rho_d \le p_{p1}\right) \end{cases} \tag{11}$$

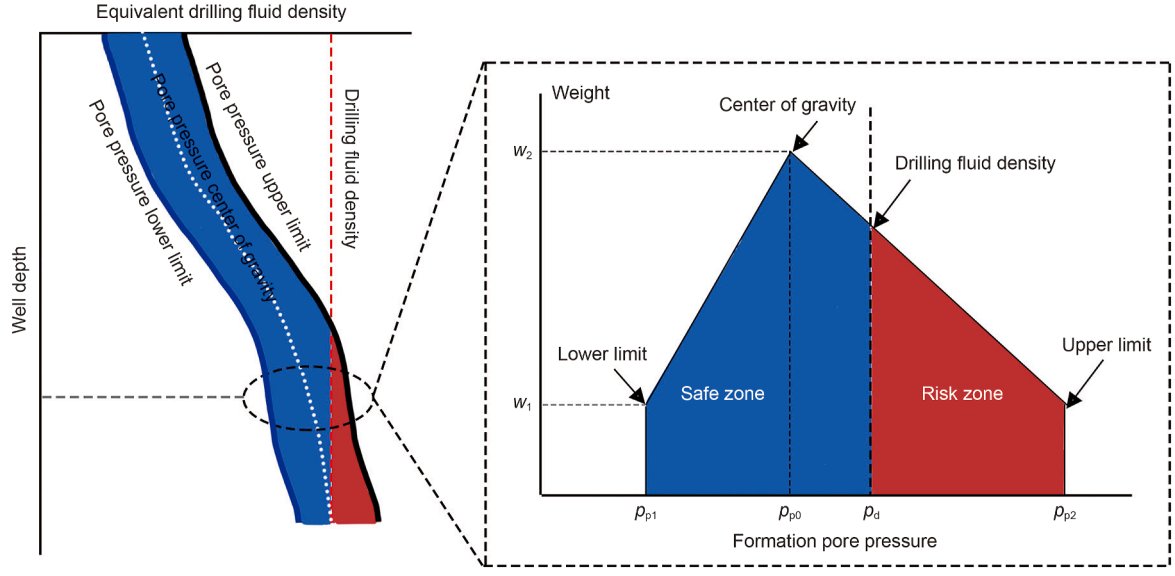

Fig. 4. Schematic diagram of overflow risk probability calculation.

within the overall distribution. Therefore, the corresponding collapse risk probability calculation model is presented in Eq. (12).

$$P = P(\rho_d < p_c) = \frac{S_{risk}}{S_{safe} + S_{risk}} = \frac{\int_{p_d}^{p_{c2}} f(p_c)\,dp_c}{\int_{p_{c1}}^{p_{c2}} f(p_c)\,dp_c}$$
$$= \begin{cases} 0 \quad (p_{c2} \le \rho_d) \\ \dfrac{\left[\dfrac{w_2 - w_1}{p_{c0} - p_{c2}}(\rho_d - p_{c0}) + w_2 + w_1\right](p_{c2} - \rho_d)}{(w_1 + w_2)(p_{c2} - p_{c1})} \times 100\% \quad (p_{c0} < \rho_d < p_{c2}) \\ \left\{\dfrac{p_{c2} - p_{c0}}{p_{c2} - p_{c1}} + \dfrac{\left[\dfrac{w_2 - w_1}{p_{c0} - p_{c1}}(\rho_d - p_{c0}) + w_2 + w_2\right](p_{c0} - \rho_d)}{(w_1 + w_2)(p_{c2} - p_{c1})}\right\} \times 100\% \quad (p_{c1} < \rho_d \le p_{c0}) \\ 100 \quad (\rho_d \le p_{c1}) \end{cases} \tag{12}$$

The other scenario involves drilling risks occurring when the drilling fluid density exceeds the upper limit of the safe drilling fluid density window, such as lost circulation and stuck pipe. Taking lost circulation risk as an example, assume that the formation fracture pressure is represented as a three-parameter interval grey number that follows a probability density function $f(p_f)$, where the upper and lower limits indicate the range of formation fracture pressure values, and the centroid represents the most likely value of the formation fracture pressure. p_{f1} represents the lower limit of the formation fracture pressure, p_{f2} represents the upper limit, and p_{f0} represents the centroid (the most likely value). p_d denotes the actual value of the drilling fluid density.

As shown in Fig. 6, on the right side of the drilling fluid density line, where the drilling fluid density is less than the formation fracture pressure, it forms a safety domain S_{safe} with a lower likelihood of lost circulation. On the left side of the drilling fluid density line, where the drilling fluid density exceeds the formation fracture pressure, the integral area S_{risk} quantifies the potential probability of lost circulation.

In the figure, the vertical axis represents the probability density function $f(p_f)$. The closer the pressure value is to p_{f0}, the greater the corresponding w, indicating a higher probability of occurrence

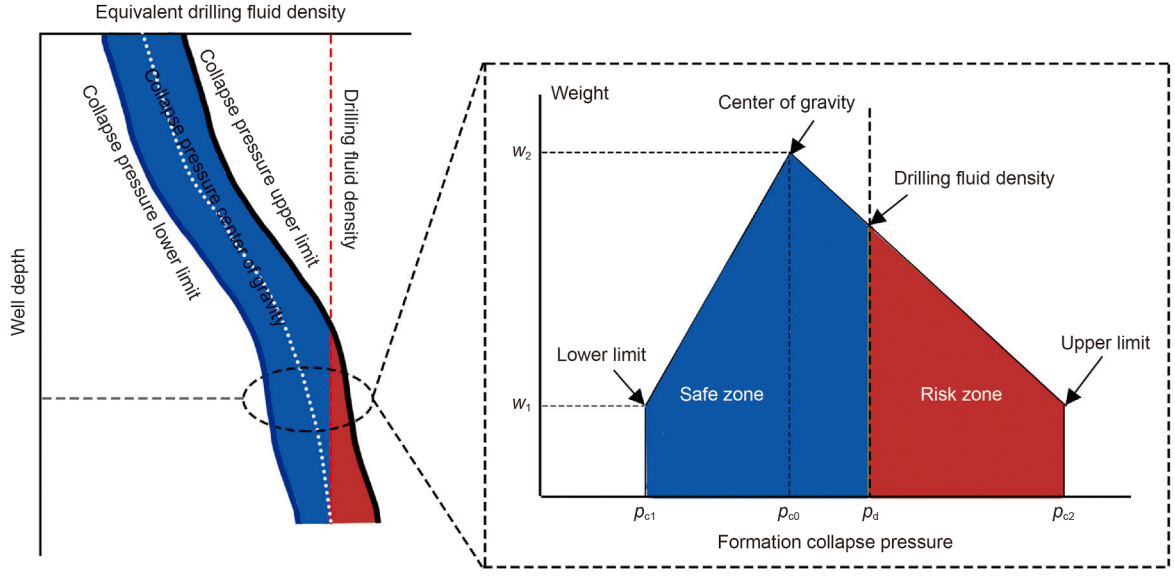

Fig. 5. Schematic diagram of collapse risk probability calculation.

within the overall distribution. Therefore, the corresponding lost circulation risk probability calculation model is presented in Eq. (13).

$$P = P\left(\rho_d > p_f\right) = \frac{S_{risk}}{S_{safe} + S_{risk}} = \frac{\int_{p_{f1}}^{p_d} f\left(p_f\right)\,dp_f}{\int_{p_{f1}}^{p_{f2}} f\left(p_f\right)\,dp_f}$$

$$= \begin{cases} 0 \quad \left(\rho_d \le p_{f1}\right) \\ \dfrac{\left[\dfrac{w_2 - w_1}{p_{f0} - p_{f2}}\left(\rho_d - p_{f0}\right) + w_2 + w_1\right]\left(p_{f2} - \rho_d\right)}{\left(w_1 + w_2\right)\left(p_{f2} - p_{f1}\right)} \times 100\% \quad \left(p_{f1} < \rho_d < p_{f0}\right) \\ \left\{\dfrac{p_{f0} - p_{f1}}{p_{f2} - p_{f1}} + \dfrac{\left[\dfrac{w_2 - w_1}{p_{f0} - p_{f2}}\left(\rho_d - p_{f0}\right) + w_2 + w_2\right]\left(\rho_d - p_{f0}\right)}{\left(w_1 + w_2\right)\left(p_{f2} - p_{f1}\right)}\right\} \times 100\% \quad \left(p_{f0} < \rho_d < p_{f2}\right) \\ 100 \quad \left(p_{f2} \le \rho_d\right) \end{cases} \tag{13}$$

For the risk of stuck pipe, assume that the formation stuck pipe pressure is represented as a three-parameter interval grey number that follows a probability density function $f(p_j)$, where the upper and lower limits indicate the range of formation stuck drilling values, and the centroid represents the most likely value of the formation stuck drilling pressure. p_{j1} represents the lower limit of the formation stuck drilling pressure, p_{j2} represents the upper limit, and p_{j0} represents the centroid (the most likely value). p_d denotes the actual value of the drilling fluid density. A schematic diagram for the calculation of stuck pipe risk probability is shown in Fig. 7.

In the figure, the vertical axis represents the probability density function $f(p_j)$. The closer the pressure value is to p_{j0}, the greater the corresponding w, indicating a higher probability of occurrence within the overall distribution. Therefore, the

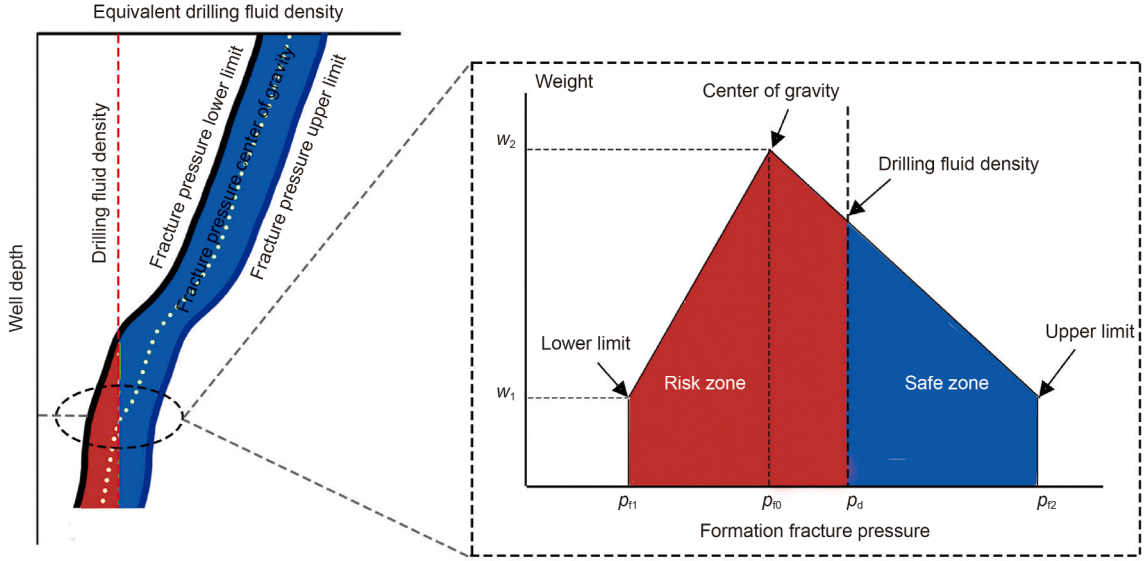

Fig. 6. Schematic diagram of lost circulation risk probability calculation.

corresponding stuck pipe risk probability calculation model is presented in Eq. (14).

$$P = P\left(\rho_d > p_j\right) = \frac{S_{risk}}{S_{safe} + S_{risk}} = \frac{\int_{p_{j1}}^{p_d} f\left(p_j\right) \mathrm{d}p_j}{\int_{p_{j1}}^{p_{j2}} f\left(p_j\right) \mathrm{d}p_j}$$
$$= \begin{cases} 0 \quad \left(\rho_d \le p_{j1}\right) \\ \dfrac{\left[\dfrac{w_2 - w_1}{p_{j0} - p_{j2}}\left(\rho_d - p_{j0}\right) + w_2 + w_1\right]\left(p_{j2} - \rho_d\right)}{\left(w_1 + w_2\right)\left(p_{j2} - p_{j1}\right)} \times 100\% \quad \left(p_{j1} < \rho_d < p_{j0}\right) \\ \left\{\dfrac{p_{j0} - p_{j1}}{p_{j2} - p_{j1}} + \dfrac{\left[\dfrac{w_2 - w_1}{p_{j0} - p_{j2}}\left(\rho_d - p_{j0}\right) + w_2 + w_2\right]\left(\rho_d - p_{j0}\right)}{\left(w_1 + w_2\right)\left(p_{j2} - p_{j1}\right)}\right\} \times 100\% \quad \left(p_{j0} < \rho_d < p_{j2}\right) \\ 100 \quad \left(p_{j2} \le \rho_d\right) \end{cases} \tag{14}$$

Based on the formation pressure variation with depth diagram, the pressure parameters at different depths, including the upper and lower limits and the centroid of pore pressure, collapse pressure, and fracture pressure, can be analyzed to obtain the safe drilling fluid density window at various depths. The pressure curves reflect the formation pressure conditions at different depths and provide a basis for selecting the appropriate drilling fluid density. By analyzing these pressure curves, it can be determined that the drilling fluid density must remain within the safe window at different depths to avoid the risks of overflow and wellbore collapse caused by low density, as well as lost circulation and stuck pipe caused by excessive density.

3. Geometric construction method for optimizing wellbore structure design

The approach to wellbore structure design is based on acquiring two pressure profile datasets. Using these datasets as the foundation and following established principles, the casing levels and the depth of casing setting for each layer are determined, either from the top down or from the bottom up, starting from the gradient of the maximum formation pressure throughout the well. In the process of wellbore structure design, designers must adhere

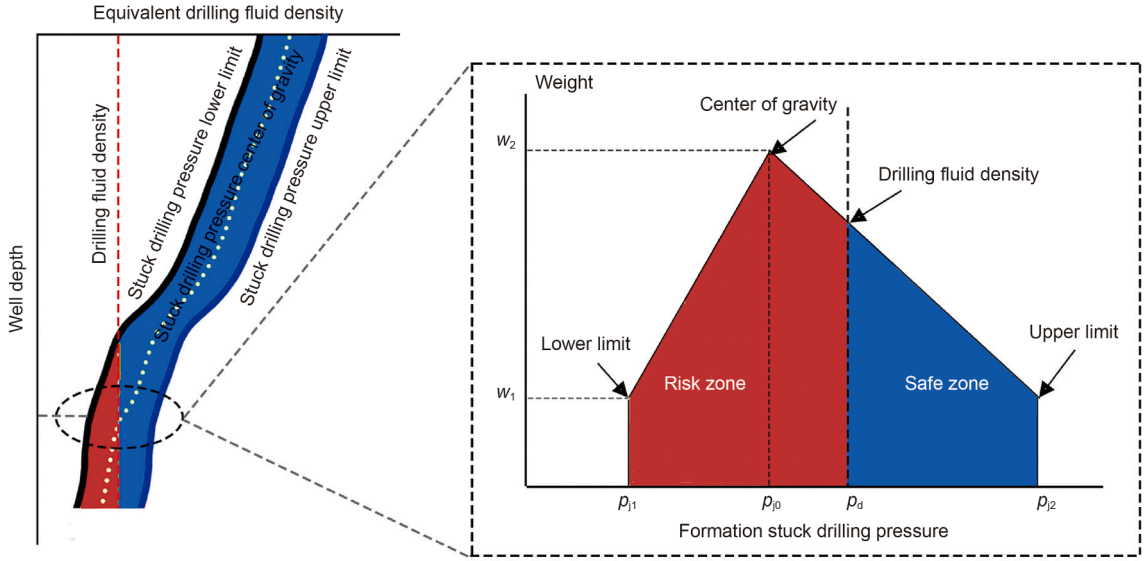

Fig. 7. Schematic diagram of stuck pipe risk probability calculation.

to the principle of working layer by layer from the inside out. Among these, the design of the intermediate casing is particularly critical, serving as the core of the entire design. Designers must ensure that the casing structure meets the requirements of development drilling and strive to minimize incidents caused by improper casing design.

For wells with uncertain pressure information, the probability distribution state of parameters in the formation pressure prediction model is determined by using the probability analysis method. Through theoretical calculation or the Monte Carlo method, a formation pressure profile with credibility is obtained (Vershkov et al., 2015). According to the pressure constraint criteria, combined with the grey number theory and the geometric construction method, a safety drilling fluid density window with credibility is constructed. On this basis, a top-down and bottom-up wellbore structure design method is proposed. Through the upper limit, lower limit and centroidal parameters of the grey number, three path designs are formed, respectively realizing the wellbore structure design schemes of the safest, most economical and most balanced. The safest scheme gives priority to the safety margin in wellbore structure design (Lodi and Grasso, 2018), which is suitable for complex formation conditions. The most economical scheme is based on the need to reduce construction costs and optimize resource allocation. The most balanced scheme takes into account both safety and economy, and is suitable for the design needs of achieving a balance between risks and benefits. Through these methods, the repeated trial-and-error process of shut-in well kicks and differential pressure sticking depths in the traditional design is avoided, making the determination of casing levels and depths more efficient, continuous and scientific, and improving the reliability and practicability of wellbore structure design.

3.1. The bottom-up geometric construction design method

The bottom-up design method starts from the bottom of the well and gradually determines the setting depth of each casing layer moving upward. First, the setting depth of the production casing is determined, ensuring it meets the requirements for development drilling. Then, based on the maximum value of the lower boundary of the safe window above the previous casing, the setting depths of the upper casings are determined step by step, up to the wellhead. This method is suitable for deep or geologically complex formations and is particularly effective in ensuring the safety of the wellbore structure under high-pressure or highly variable pressure conditions. To further optimize the wellbore structure design, a bottom-up grey-number band for drilling fluid density is established, taking into account the variation of drilling fluid density at different depths, as shown in Fig. 8.

In the schematic diagram of the grey-number band for the upper and lower limits of drilling fluid density, L_{j0} and L_{j1} represent the lower and upper bounds of the grey-number band for the lower limit of drilling fluid density, respectively; H_{j0} and H_{j1} represent the lower and upper bounds of the grey-number band for the upper limit of drilling fluid density, respectively. Within the grey-number band, L_{j*} and H_{j*}, representing the maximum probable values based on grey information, are introduced to optimize the wellbore structure design and ensure more accurate casing setting depths. As shown in Fig. 9, a bottom-up wellbore structure design was carried out using the geometric construction method, resulting in three feasible design schemes.

After determining the design well depth D_1 as the setting depth of the production casing, the wellbore structure design is carried out according to the following steps:

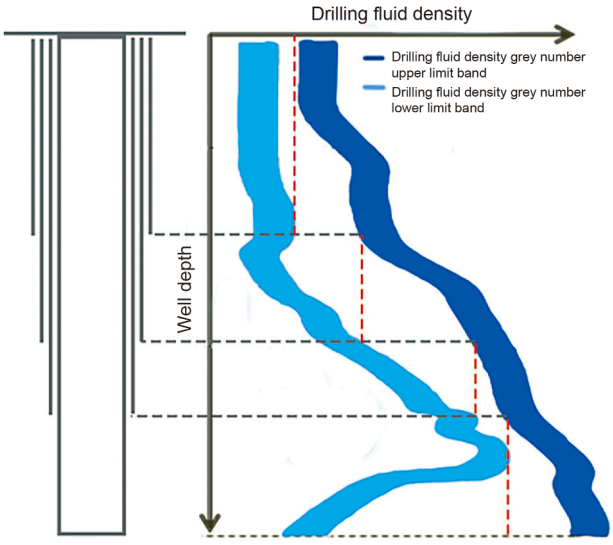

Fig. 8. Schematic diagram of the bottom-up design method.

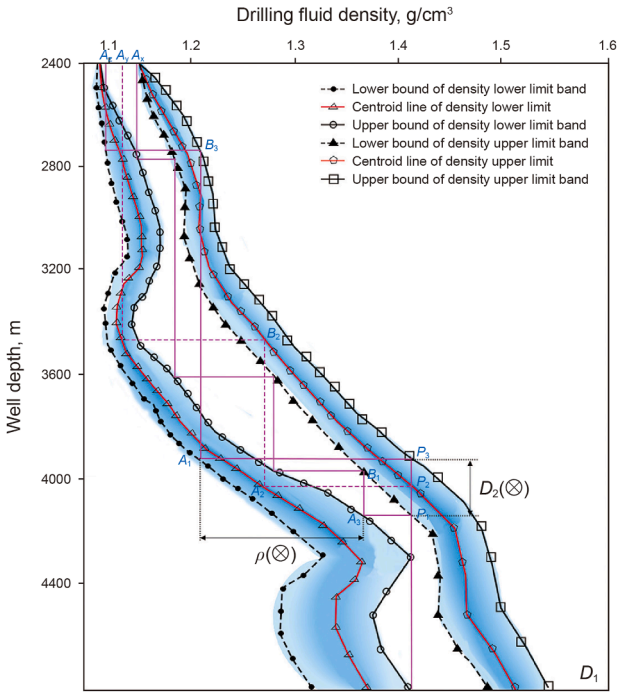

Fig. 9. Application of the geometric construction method in bottom-up wellbore structure design.

1) Determine the grey number for the setting depth of the deepest technical casing. Due to the higher formation pressure and temperature in deeper formations, the associated drilling risks are relatively greater. Therefore, in the wellbore structure design, the upper bound of the grey number for the lower limit of the drilling fluid density is prioritized to ensure a higher safety margin in deeper sections. A vertical line is drawn upward from the maximum value of the upper bound, intersecting H_{j0}, H_{j*}, and H_{j1} at points P_1, P_2, and P_3, respectively. The vertical coordinates of these three points represent the grey number for the setting depth of the deepest technical casing, $D_2(\otimes)\in(D_{22}, D_2{*}, D_{21})$.

2) Determine the grey number for drilling fluid density. Draw a horizontal line at the setting depth grey number $D_2(\otimes)$ of the deepest technical casing. This line intersects L_{j0}, L_{j*}, and L_{j1} at points A_1, A_2, and A_3, respectively. The horizontal coordinates of these points determine the grey number for drilling fluid density as $\rho(\otimes)\in(\rho_0, \rho^*, \rho_1)$. Similarly, the horizontal line intersects H_{j0}, H_{j*}, and H_{j1} at points B_1, B_2, and B_3. Based on these intersections, the grey number for the setting depth of the next upper technical casing is determined as $D_3(\otimes)\in(D_{32}, D_3^*, D_{31})$.
3) By repeating the above steps, the upper technical casings and surface casing can be determined, completing the wellbore structure design up to the wellhead.
4) Construct node paths. The boundary nodes of the casing setting depth grey numbers and the drilling fluid density grey numbers obtained from the above steps are connected to construct the design paths. The path P_1-A_3-B_1 … -A_x represents the safest wellbore structure design scheme. The path P_2-A_2-B_2 … -A_y represents the balanced grey-number wellbore structure design scheme, while the path P_3-A_1-B_3 … -A_z represents the most economical wellbore structure design scheme.

The bottom-up programmatic design of wellbore structure (Yang et al., 2017) is illustrated through the design flowchart shown in Fig. 10. The flowchart is divided into several key steps, which are used to implement the sectional design of the wellbore structure and allow for the selection among different design paths (safe, balanced, or economical).

1) Initialization. First, initialize the upper and lower limit arrays of the grey number for drilling fluid density. H, Pl, and Pu represent the depth and the upper and lower limits of the density window, respectively. Additionally, set the initial layer number $k = 1$, and assign $Hc[k]$ as the initial depth $H[i]$. Initialize the variables i and j to the depth of the well bottom N, and set P_{max} and P_{min} as the lower and upper bounds of the grey number for drilling fluid density at the well bottom ($Pl[N]$ and $Pu[N]$).

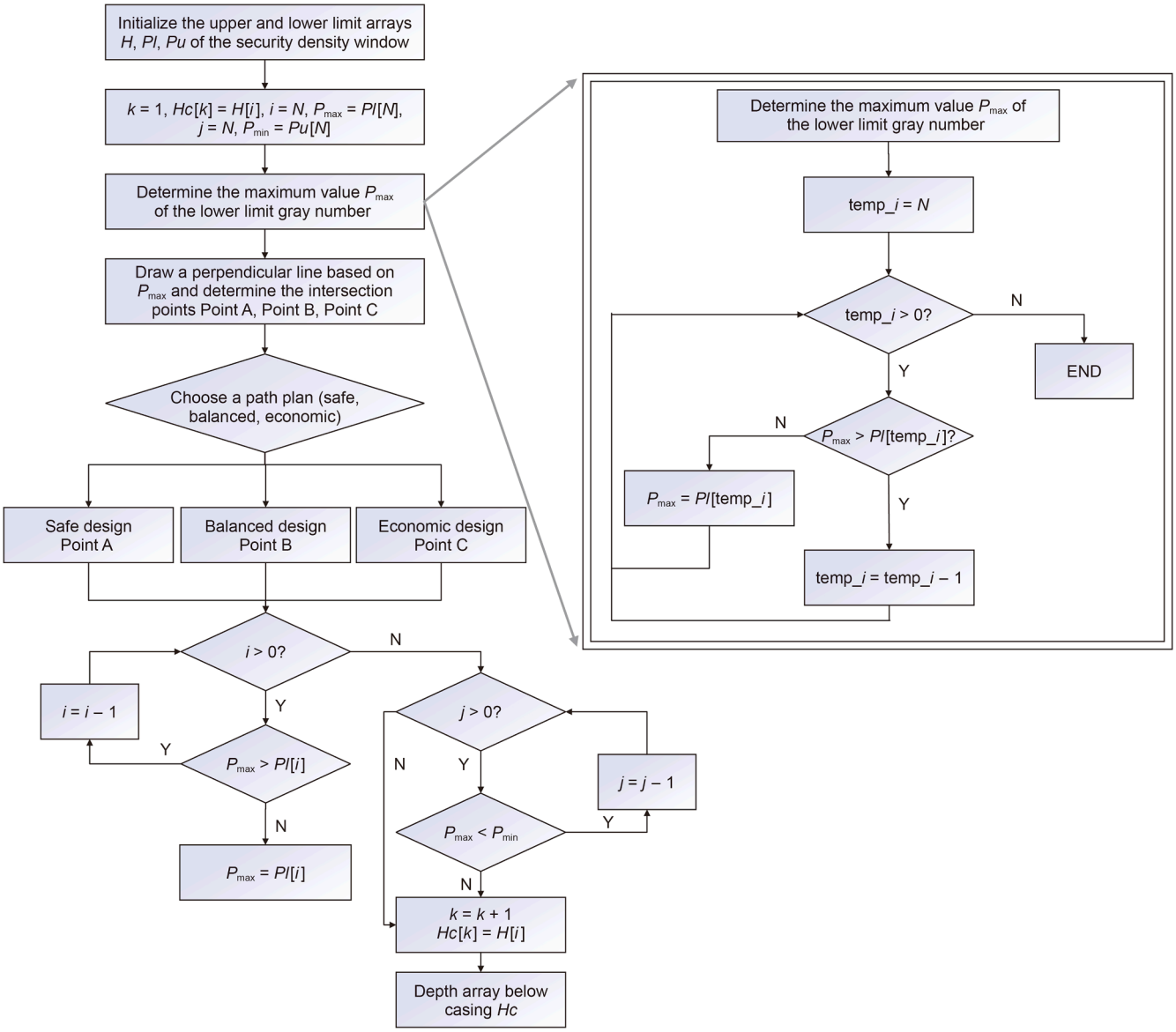

Fig. 10. Programmatic design flowchart for bottom-up wellbore structure.

2) Determine the maximum value P_{max} of the lower limit grey number. To find the maximum value P_{max} of the lower limit of the drilling fluid density grey number throughout the well depth, a separate sub-process is used. In this sub-process, the variable *temp_i* is used to traverse the *Pl* array starting from *N*.
3) Determine the intersection points according to P_{max}. Using the determined value of P_{max}, draw a vertical line and identify three intersection points: Point A, Point B, and Point C. These three points serve as the starting points for the three design paths, representing the safe design (Point A), balanced design (Point B), and economical design (Point C), respectively.
4) Inspection of the drilling fluid density range. In the circulation section, the lower limit grey number of drilling fluid density at each depth is checked layer by layer from bottom to top to ensure it does not exceed the already determined maximum lower limit value. Then, the upper limit grey number at each depth is verified to ensure that the maximum density value remains within the permissible safe range. Through this layer-by-layer inspection and updating process, the entire wellbore structure design is ensured to meet the requirements of the safe density window.
5) Update the number of layers, record the depths, and output the results.

Based on the obtained design method, the results for the bottom-up casing levels and setting depth design are shown in Table 1 (Marbun et al., 2020). Starting from D_1, the production casing, the subsequent technical casings and surface casing can then be determined.

3.2. The up-bottom geometric construction design method

The up-bottom design method starts at the wellhead and progressively determines the setting depth for each casing layer. First, the minimum value of the upper limit of the safe window at the wellhead is identified, and the casing setting depth is calculated based on the pressure constraint profile. Then, the setting depths of each subsequent casing string are determined sequentially until reaching the designed well depth. This method is suitable for shallow geological environments with stable formation pressures and lower risk. To ensure the accuracy of the wellbore structure design, an up-bottom grey number band for drilling fluid density is established, considering variations in drilling fluid density at different depths, as shown in Fig. 11.

The up-bottom geometric design method is similar to the bottom-up method. The specific process and design results are shown in Fig. 12.

1) Determine the setting depth grey number for the surface casing. Due to the low formation strength and small fracture pressure in shallow formations at the wellhead, there is a higher risk of lost circulation and wellbore instability.

Table 1
Results of bottom-up casing levels and setting depth design.

Casing levels	Setting depth grey number	Maximum probable setting depth of casing
Surface casing	$D_n(\otimes)$	D_{n^*}
Technical casing 1	$D_{n-1}(\otimes)$	$D_{(n-1)^*}$
Technical casing 2	$D_{n-2}(\otimes)$	$D_{(n-2)^*}$
⋮	⋮	⋮
⋮	⋮	⋮
Technical casing $n-2$	$D_2(\otimes)$	D_{2^*}
Production casing	D_1	

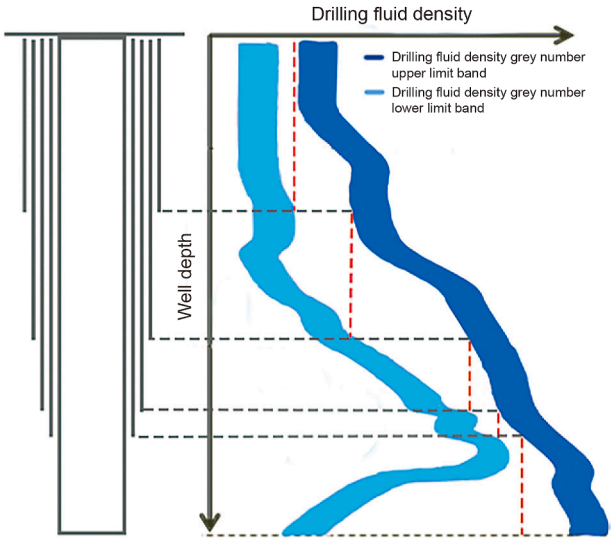

Fig. 11. Schematic diagram of the up-bottom design method.

Therefore, in the wellbore structure design, the lower bound of the grey number for the upper limit of the drilling fluid density is prioritized to reduce shallow formation pressure risks and ensure wellbore integrity. A vertical line is drawn downward from the minimum value of the lower bound, intersecting L_{j0}, L_{j*}, and L_{j1} at points P_3, P_2, and P_1, respectively. The vertical coordinates of these three points represent the grey number for the setting depth of the surface casing, $D_1(\otimes) \in (D_{11}, D_{1*}, D_{12})$.
2) Determine the grey number for drilling fluid density. A horizontal line is drawn at the setting depth grey number $D_1(\otimes)$ for the surface casing, intersecting H_{j0}, H_{j*}, and H_{j1} at points B_1, B_2, and B_3, respectively. The horizontal coordinates of these three

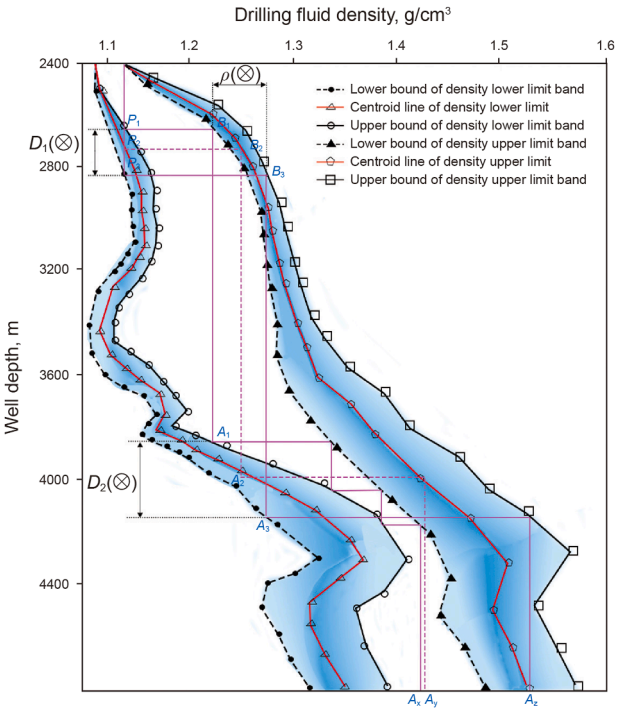

Fig. 12. Application of the geometric construction method in up-bottom wellbore structure design.

points represent the grey number for drilling fluid density $\rho_1(\otimes)\in(\rho_{11}, \rho_{1*}, \rho_{12})$. Similarly, the vertical line intersects L_{j0}, L_{j*} and L_{j1} at points A_1, A_2, and A_3. Based on these intersections, the grey number for the setting depth of the technical casing 1 is determined as $D_2(\otimes)\in(D_{21}, D_{2*}, D_{22})$.

3) By repeating the above steps, the lower technical casings can be determined, continuing the wellbore structure design down to the target depth.
4) Construct node paths (Saeed et al., 2020). The boundary nodes of the casing setting depth grey numbers and the drilling fluid density grey numbers obtained from the above steps are connected to construct the design paths. The path P_1-B_1-A_1 … -A_x represents the safest wellbore structure design scheme. The path P_2-B_2-A_2 … -A_y represents the balanced grey-number wellbore structure design scheme, while the path P_3-B_3-A_3 … -A_z represents the most economical wellbore structure design scheme.

The up-bottom programmatic design of wellbore structure is illustrated through the design flowchart shown in Fig. 13.

Based on the obtained design method, the results for the up-bottom casing levels and setting depth design are shown in Table 2.

4. Results and discussion

The Yaha Gas Storage Facility is located in Kuqa, Xinjiang, China. It is one of the deepest underground natural gas storage facilities in the country, with an average reservoir burial depth exceeding 5,100 m and some wells reaching depths beyond 5,500 m. It is a typical example of a deep, high-pressure gas reservoir converted into a gas storage site. The total storage capacity of the facility is 1.516×10^9 m^3, with a designed maximum daily gas supply capacity of up to 3.0×10^7 m^3. It plays a vital role in peak shaving, emergency supply, and ensuring stable delivery within the West-

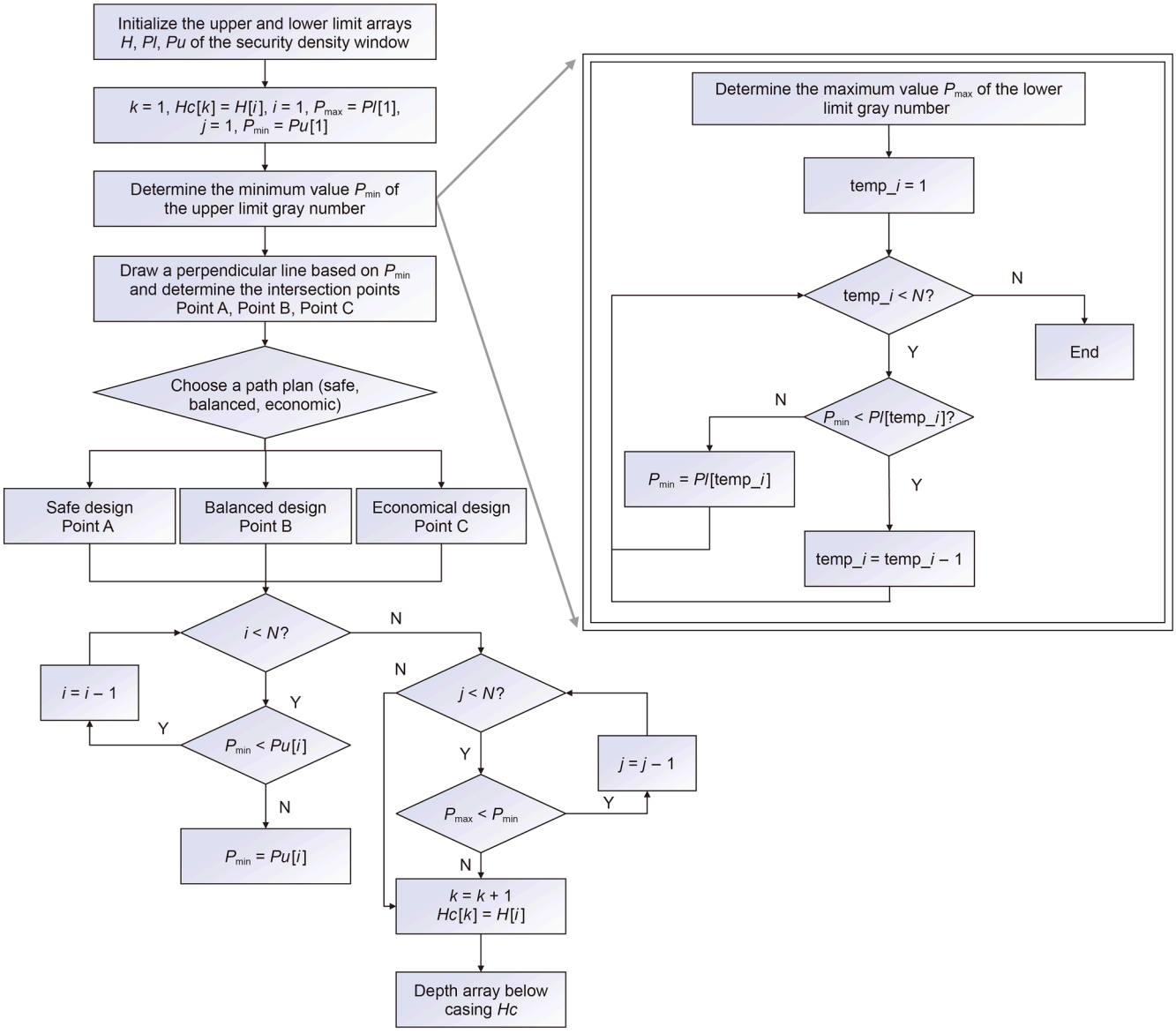

Fig. 13. Programmatic design flowchart for up-bottom wellbore structure.

Table 2
Results of up-bottom casing levels and setting depth design.

Casing levels	Setting depth grey number	Maximum probable setting depth of casing
Surface casing	$D_1(\otimes)$	D_{1*}
Technical casing 1	$D_2(\otimes)$	D_{2*}
Technical casing 2	$D_3(\otimes)$	D_{3*}
⋮	⋮	⋮
⋮	⋮	⋮
Technical casing $n-2$	$D_{n-1}(\otimes)$	$D_{(n-1)*}$
Production casing	D_n	

East Gas Pipeline network. Due to the great depth and high pressure, the reservoir conditions differ significantly from those of shallow gas storage sites, posing more severe challenges for wellbore structure design, operational safety, and long-term stability.

The geological conditions in the area where this gas storage facility is located are complex and variable. The formations are primarily composed of interbedded deep dolomite, sandstone, shale, and mudstone. Some reservoir sections feature fracture-developed zones, resulting in uneven formation stress distribution, which increases the likelihood of wellbore collapse and casing deformation (Zhang et al., 2022). These intricate geological conditions pose significant challenges to the design and construction of the gas storage facility, particularly in the wellbore structure design, where the following key issues are encountered:

1) Extreme high pressure and large pressure gradient variations: Due to its burial depth far exceeding that of conventional gas storage facilities, the reservoir pressure of the Yaha Gas Storage Facility is extremely high, reaching 70–100 MPa, and exhibits significant pressure gradient variations. There are substantial differences in pore pressure and fracture pressure across different well depths, resulting in an extremely narrow drilling fluid density window. Even slight deviations may lead to lost circulation or blowouts. This necessitates highly accurate prediction and control of drilling fluid density to prevent safety incidents such as lost circulation or blowouts.
2) Complex geological structures and tectonic stress: The storage area is characterized by diverse sediment types and unstable geological structures, complicating pressure prediction and drilling fluid density control during drilling operations. Additionally, the reservoir rocks are relatively hard, and the drilling process must contend with high drilling pressures, high temperatures, and complex interactions with the drilling fluid. Effectively monitoring and adjusting the drilling fluid density to ensure wellbore structural safety and operational stability is a key challenge in the design of the storage facility.
3) High requirements for wellbore structure design: The wellbore structure of the Yaha Gas Storage Facility must meet extremely stringent safety and economic standards. The design must account not only for long-term gas storage capacity but also for maintaining stable operation under high pressure and complex geological conditions, thereby avoiding catastrophic failures.

To ensure the safety and cost-effectiveness of gas storage wellbore structures, the primary objectives of this case study are as follows:

1) A three-parameter safe drilling fluid density window, comprising upper limit, lower limit, and centroid, is constructed using the centroid method in grey information theory. Based on geological exploration and historical data, the upper and lower bounds, along with the centroid values of geological parameters, are determined to enhance the accuracy of the density window. Data from adjacent wells are referenced during calculations to improve the reliability of the results.
2) Applying the three-parameter safe drilling fluid density window to the design of gas storage wellbore structures. Using the three-parameter safe drilling fluid density window, a geometrical mapping design method is employed from bottom to top and top to bottom to ensure safety requirements are met while achieving greater economic benefits.
3) Validating the model's effectiveness through a real-world case study. Real data is input into the model for risk assessment and analysis, followed by a comparison with actual design and construction outcomes to verify the model's validity and reliability.

In a specific structural area of the Kuqa region, a key development well, WO, was drilled to a final depth of 6,130 m. Due to the mismatch between the drilling fluid density and the safe drilling fluid density window, multiple drilling risks occurred during its construction. To address this, data from four adjacent wells in the same structural area were selected to evaluate drilling risks across all depth intervals of the WO well. Using a safety risk evaluation model, the risk probability for each depth interval was calculated, providing a reference for further optimization of the design. The actual risks of the target well and the evaluation results are shown in Table 3.

When transferring the formation information from adjacent wells to the target well, the formation pressure matrix of the adjacent wells (Fig. 14(a)) is first subjected to depth adjustment processing (Fig. 14(b)). Then, based on inverse distance weighted interpolation and the method for determining the three-parameter interval grey number, the three-parameter interval grey numbers of the formation pressure are calculated (Fig. 14(c)) and compared with the formation pressure derived from the logging interpretation of the target well.

Based on data from adjacent wells and the actual operating conditions of the target well, this study established a drilling risk evaluation model under the framework of three-parameter interval grey numbers, producing the wellbore risk matrix for the entire depth of the target well. The evaluation results, as shown in Fig. 15, indicate a high consistency between the model's calculated risk evaluation results and the actual drilling risks observed on-site, further confirming the model's reliability and applicability.

In practical engineering, to address the high overflow risk in the 3537 m well section, comprehensive analysis of offset well pressure data and risk assessment results determined that the pore pressure in the 3530–3600 m interval is approximately 66 MPa, while the fracture pressure is around 70 MPa, leaving a safe density window of less than 0.05 g/cm^3. To mitigate this, managed pressure drilling technology (MPD) was adopted, employing a rotating control device combined with a real-time choke manifold

Table 3
Actual risks of the target well and risk evaluation results.

Well depth, m	Drilling risks	Model calculation results, %
609	Lost circulation	15.5
3537	Overflow	84.5
3868	Lost circulation	85.5
4087	Stuck pipe	86.5
4289	Lost circulation	89.5
4639	Lost circulation	91
4808	Lost circulation	62
5758	Stuck pipe	42.5

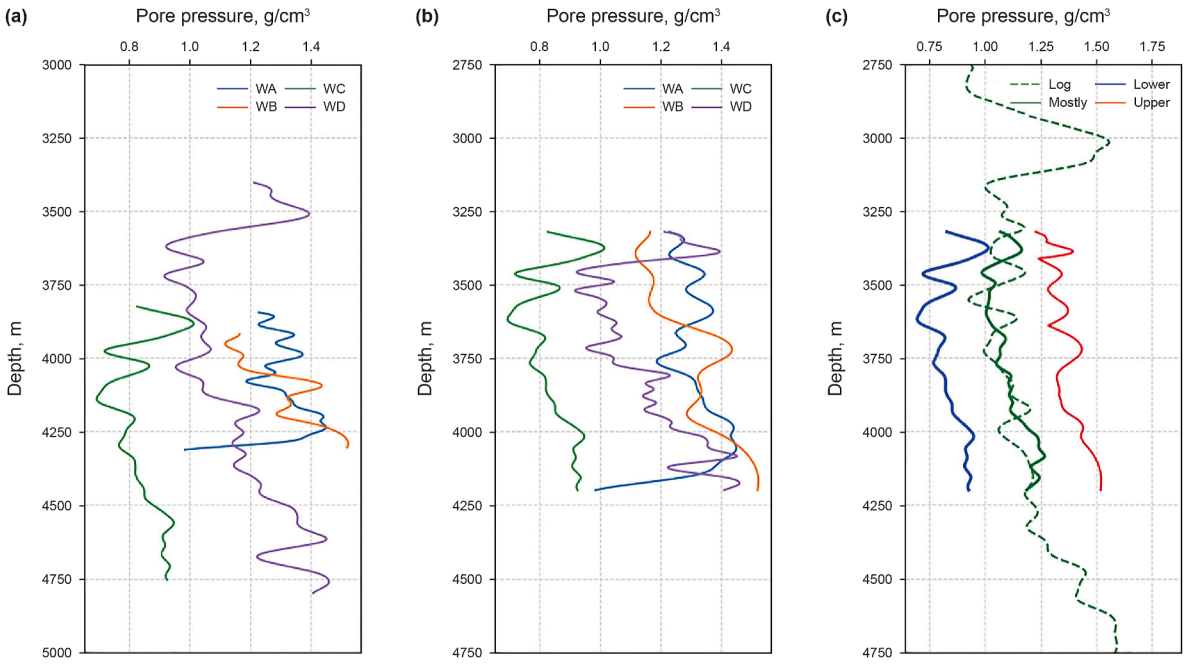

Fig. 14. Depth adjustment and formation pressure comparison. (**a**) Actual formation pressure of adjacent wells. (**b**) Depth-adjusted formation pressure of adjacent wells. (**c**) Grey numbers and actual formation pressure of the target well.

backpressure control system to dynamically manage bottomhole pressure. The initial drilling fluid density was set to 1.68–1.70 g/cm^3, and the backpressure was maintained within a range of 0.55–0.83 MPa. Based on real-time pressure monitoring, dynamic adjustments were made to ensure the bottomhole pressure remained within a safe range 0.5–1.0 MPa above the pore pressure and at least 2.0 MPa below the fracture pressure. Through precise control of both backpressure and drilling fluid density, effective pressure management was achieved in this ultra-high-pressure, narrow-window formation. As a result, no overflow, lost circulation, or abnormal casing pressure increase occurred during the drilling of the 3530–3600 m interval, significantly enhancing the safety and stability of the drilling process.

Although managed pressure drilling effectively controlled localized high-risk intervals, overall drilling risk still requires systematic reduction—especially under high-pressure, complex formation conditions—to provide greater safety margins for subsequent operations. To address this, this study further proposes a geometric construction method that integrates the results of risk assessment. By adjusting the drilling fluid density window and casing hierarchy design, this method aims to dynamically balance operational safety and economic efficiency. Using risk distribution evaluation results as the core basis for design optimization, the method explores multiple design pathways to comprehensively optimize the construction plan for the target well. This approach not only meets diverse safety requirements but also achieves an effective balance between safety and construction costs.

In the well design process, considering the uncertainties of formation pressure, this study proposes three different design pathway options, each corresponding to a specific design objective: highest security, a balance between safety and cost-effectiveness, and economy. The detailed characteristics of these options are as follows:

1) Safest design option: This pathway is suitable for complex formation environments with the highest risks, prioritizing the safety of the gas storage facility. It offers the highest safety margin (Zhu and Liu, 2020), with the most casing layers covering a greater depth range. However, it also involves relatively higher construction costs and is appropriate for areas with strict requirements for the long-term stability of the gas storage facility.
2) Balanced design option: This pathway is suitable for formations where risks are manageable, aiming to strike a balance between safety and cost-effectiveness. It provides a moderate safety margin by reducing some casing layers with a moderate depth range. This design meets the routine safety requirements of gas storage facilities while controlling costs.

Table 4
Comparison of wellbore structure design schemes.

Scheme type	Casing levels	Safety margin	Construction cost
Safest design	4	High	High
Balanced design	3	Moderate	Moderate
Economical design	2	Low	Low

Table 5
Design results of casing layers and bottom depth of different design schemes.

Safest design	Depth 1, km	Balanced design	Depth 2, km	Economical design	Depth 3, km
Surface casing	0.000–0.460	Surface casing	0.000–0.480	Surface casing	0.000–0.490
Technical casing 1	0.460–4.800	Technical casing 1	0.480–4.900	Production casing	0.490–5.200
Technical casing 2	4.800–5.600	Production casing	4.900–5.900		
Production casing	5.600–6.000				

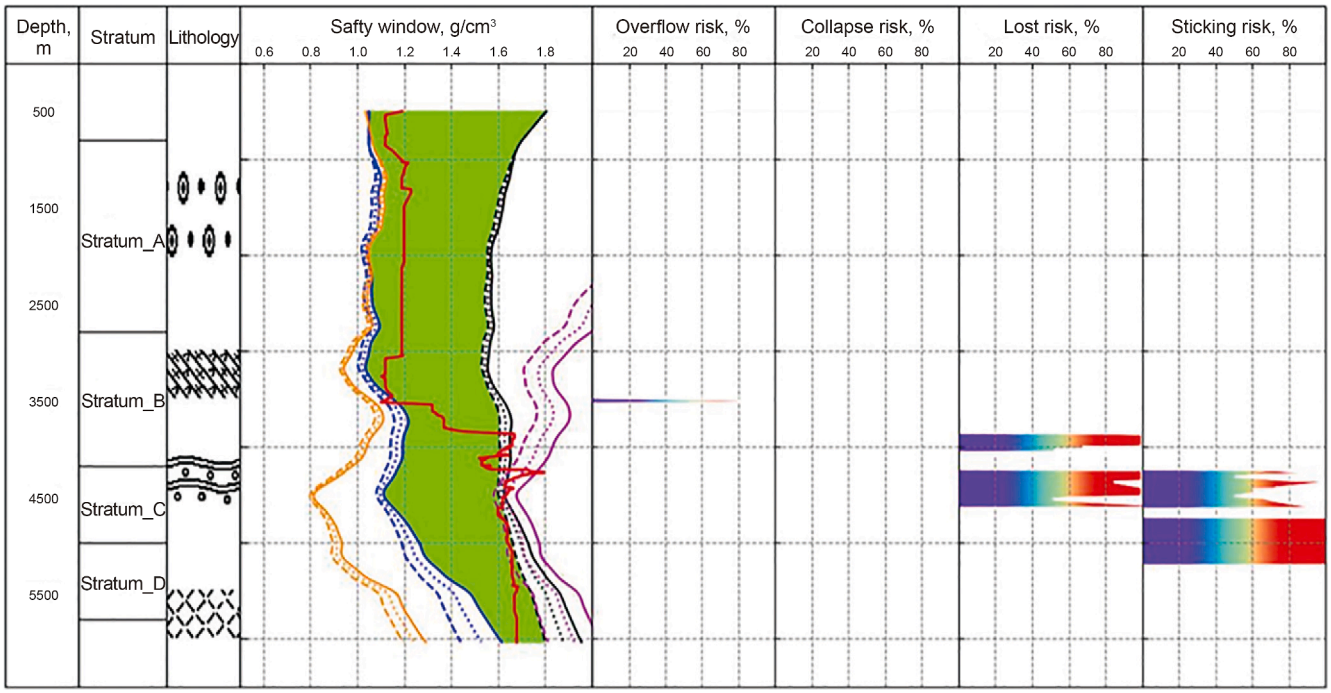

Fig. 15. Drilling risk evaluation results of the target well.

3) Economical design option: This pathway is suitable for regions with relatively low risks, where economic considerations are prioritized. It features the lowest safety margin, with the fewest casing layers and the smallest depth range. This design minimizes construction costs and is applicable to scenarios with stable formations and low safety requirements.

Through the optimization design using the geometric construction method, the three design pathways dynamically adjust the casing levels and depth range to meet different design requirements. A comprehensive comparison was conducted regarding casing layers, depth range, safety margin, and construction cost across the different design pathways. The design results are shown in Tables 4 and 5.

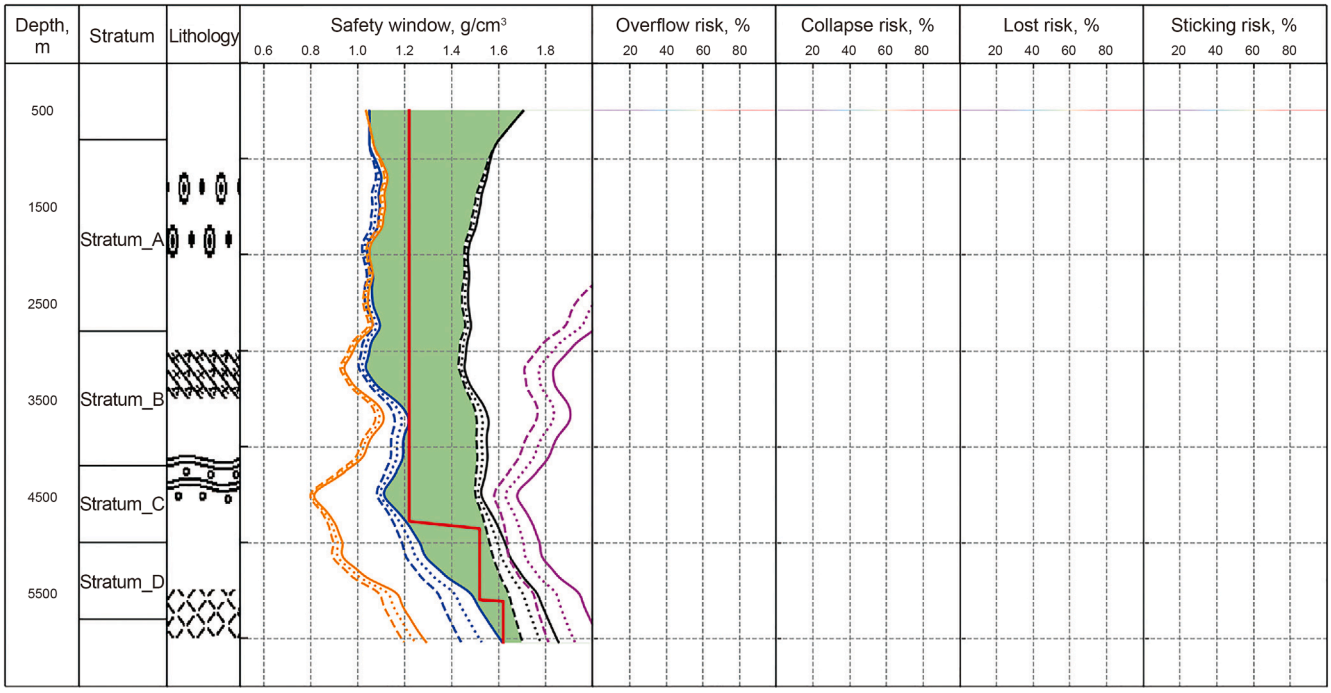

Fig. 16. Drilling risk evaluation results under the safest design scheme.

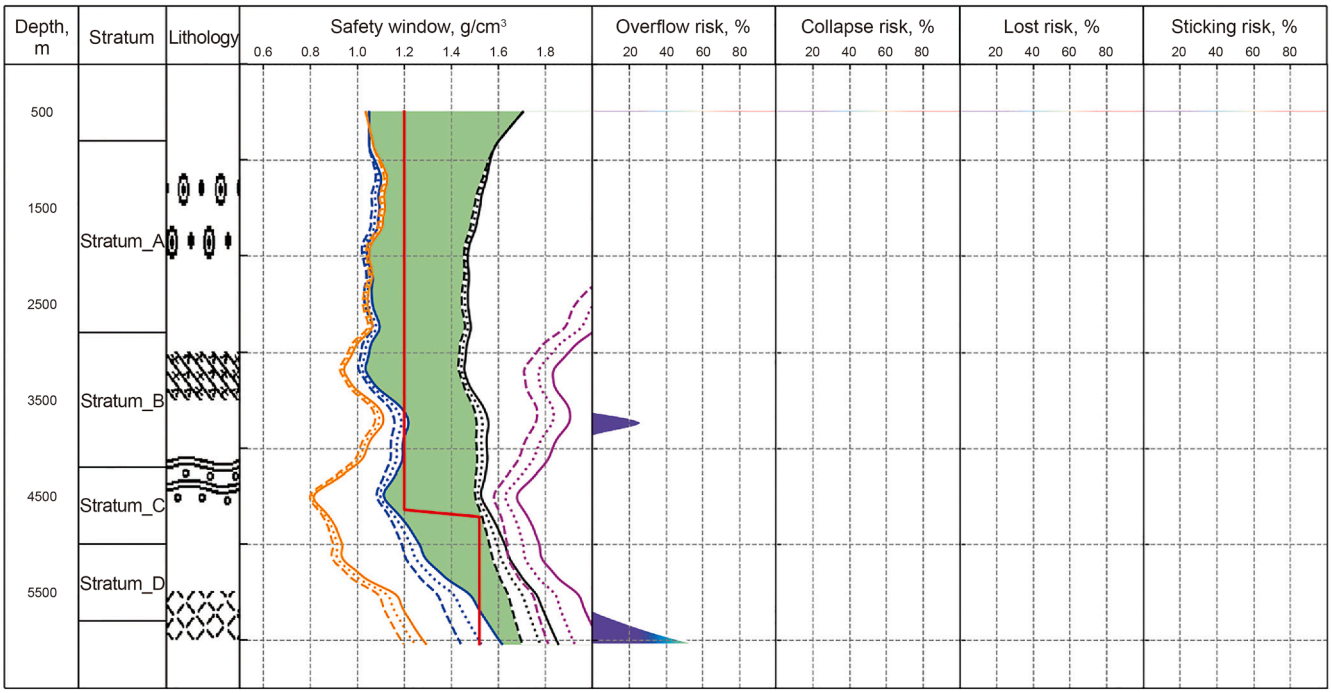

Fig. 17. Drilling risk evaluation results under the balanced design scheme.

Based on the three-parameter interval grey number and the geometric construction design method, the drilling risks of the three wellbore structure design schemes were evaluated programmatically. The evaluation results are shown in Figs. 16–18.

During the actual construction process, the target well adopted the casing levels and depth range shown in Table 6. The actual results aligned with the casing levels and depth range of the maximum safety design scheme in Table 5, demonstrating the accuracy of the design method. As observed in Table 6, the actual casing levels and depth range fall within the designed range, where the determination of the conductor casing depth was primarily based on wellhead load-bearing capacity.

The results of this case study demonstrate that, by integrating drilling risk assessment with MPD and geometric mapping-based

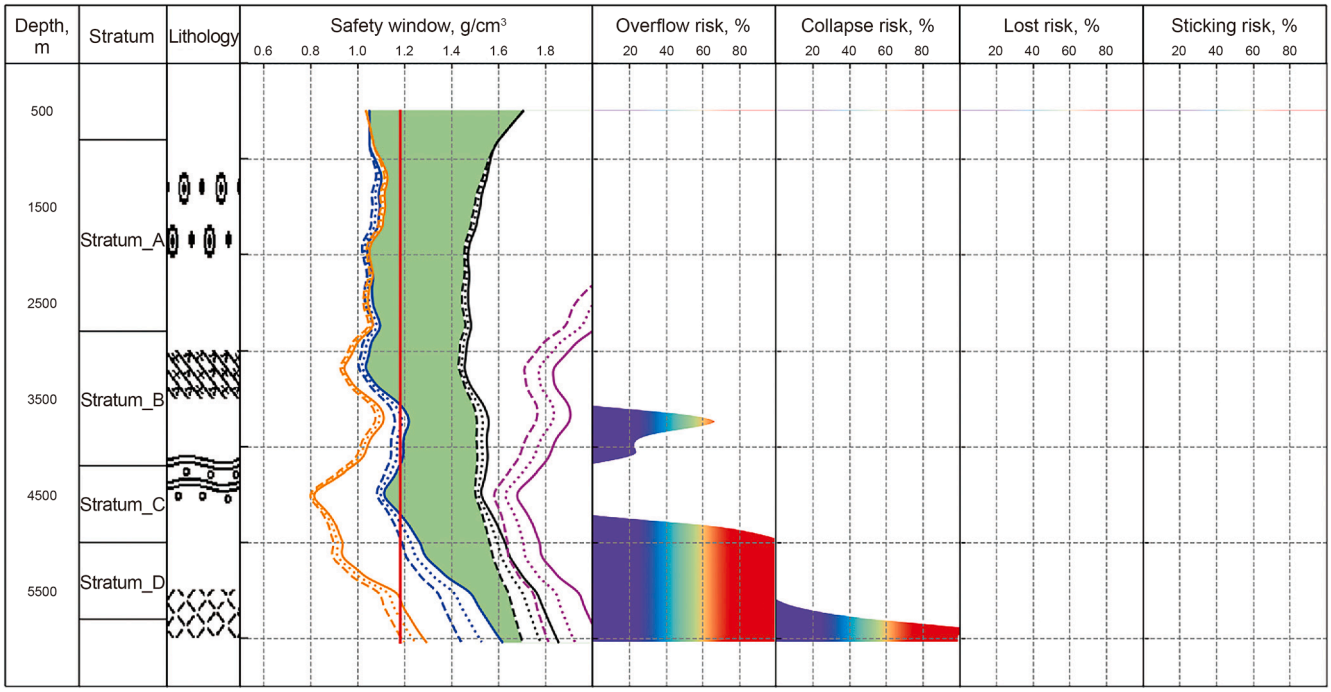

Fig. 18. Drilling risk evaluation results for the economical design scheme.

Table 6
Actual wellbore structure of the target well.

Wellbore size d_w, mm	Casing types	Casing size d_c, mm	Depth, km
660.4	Conductor pipe	914.4	0.0294
660.4	Surface casing	508	0.0471
444.5	Technical casing 1	346	4.8250
269.9	Production casing	244.5	5.8686

optimization of wellbore structure design, both the safety and cost-efficiency of the well can be significantly improved. This approach also provides a scientific basis for the design of wellbore structures in similarly complex gas storage reservoirs. In practical implementation, a balanced wellbore structure design was selected, and managed pressure drilling was applied in ultra-deep sections to successfully control the overflow risk in ultra-high-pressure, narrow-window formations. This ensured high safety standards while effectively managing construction costs. However, the application of MPD in ultra-deep sections also highlights areas for further improvement in the current design, offering directions for future optimization. This study provides a flexible and reliable reference for the design of gas storage wellbore structures under varying risk levels.

5. Conclusions

1) This paper proposes a risk-based wellbore structure design method for gas storage reservoirs based on grey geological information. By constructing a three-parameter safe drilling fluid density window comprising the upper limit, lower limit, and centroid, the method effectively addresses geological uncertainty in complex formations and enhances the precision and reliability of wellbore structure design.
2) Based on the full-well pressure profile data, both up-bottom and bottom-up geometric construction design methods were employed to design the casing setting depths. Three design paths are proposed, fulfilling the requirements for the safest, most economical, and most balanced wellbore structure designs, thereby enhancing the flexibility and engineering adaptability of the well design.
3) The practical application in the Yaha Gas Storage Facility validated that the model's predicted risk distribution closely matched actual drilling conditions, fully demonstrating the method's applicability and scientific soundness under incomplete geological information. It also highlights its strong engineering practicality and potential for broader application.
4) While effective under complex geological conditions, the method still depends on accurate geological parameters and a stable drilling fluid density window. Future integration of multi-source data, intelligent algorithms, and a smart design platform combining risk assessment and optimization will enhance its applicability.

CRediT authorship contribution statement

Kai Wei: Writing – review & editing, Writing – original draft, Methodology, Funding acquisition. **Zhe Xu:** Writing – original draft, Software, Conceptualization. **Ao Cai:** Software, Data curation. **Yan-Xian Wu:** Data curation, Conceptualization. **Yan Yan:** Funding acquisition, Data curation, Conceptualization.

Availability of data and materials

Data will be made available on request.

Declaration of competing interest

The authors declare that they have no known competing financial interests or personal relationships that could have appeared to influence the work reported in this paper.

Acknowledgements

This work received funding from the National Natural Science Foundation of China (52174017), the Open Fund of the Key Laboratory of Deep Geothermal Resources (Ministry of Natural Resources, China University of Geosciences, Wuhan) (KLDGR2022G05), the Open Fund of the Hubei Key Laboratory of Drilling and Production Engineering for Oil and Gas (Yangtze University) (YQZC202104) and the Youth Project funded by Shanxi Province Natural Science Basic Research Program (2024JC-YBQN-0522). The authors would like to express their sincere gratitude to the anonymous reviewers for their constructive comments and valuable suggestions, which greatly improved the quality of this manuscript.

References

Diaz, M.B., Kim, K.Y., 2020. Improving rate of penetration prediction by combining data from an adjacent well in a geothermal project. Renew. Energy 155, 1394–1400. https://doi.org/10.1016/j.renene.2020.04.029.
Du, S., Bai, M., Shi, Y., Zha, Y., Yan, D., 2024. A review of the utilization of CO_2 as a cushion gas in underground natural gas storage. Processes 12 (7), 1489. https://doi.org/10.3390/pr12071489.
Guan, Z., Li, C., Zhou, G., et al., 2001. Well structure design method of deep and ultra-deep wells. J. Univ. Pet., China (Ed. Nat. Sci.) 25 (6), 42–44. https://doi.org/10.3321/j.issn:1000-5870.2001.06.012 (in Chinese).
He, D., Wang, L., Ji, G., Wei, Y., Jia, C., 2012. Well spacing optimization for Sulige tight sand gas field, NW China. Petrol. Explor. Dev. 39 (4), 491–497. https://doi.org/10.1016/S1876-3804(12)60066-4.
Hong, D., Tang, X., Gao, W., Mao, W., Wang, P., Liu, K., 2020. A new calculation approach of wellbore separation factor based on the relative position of adjacent wells. Petrol. Explor. Dev. 47, 196–203. https://doi.org/10.1016/S1876-3804(20)60018-0.
Hoseinpour, M., Riahi, M.A., 2022. Determination of the mud weight window, optimum drilling trajectory, and wellbore stability using geomechanical parameters in one of the iranian hydrocarbon reservoirs. J. Pet. Explor. Prod. Technol. 12, 63–82. https://doi.org/10.1007/s13202-021-01399-5.
Hu, W., Xia, W., Li, Y., Jiang, J., Li, G., Chen, Y., 2022. An intelligent identification method of safety risk while drilling in gas drilling. Petrol. Explor. Dev. 49 (2), 428–437. https://doi.org/10.1016/S1876-3804(22)60036-3.
Hund, G.E., 1986. The fault of uncertainty: geologic information in regulatory decision making. Sci. Technol. Hum. Val. 11 (4), 45–54. https://doi.org/10.1177/016224398601100405.
Iwaszczuk, N., Zapukhliak, I., Iwaszczuk, A., Dzoba, O., Romashko, O., 2022. Underground gas storage facilities in Ukraine: current state and future prospects. Energies 15 (18), 6604. https://doi.org/10.3390/en15186604.
Jiang, T., Wang, Z., Wang, J., 2021. Integrated construction technology for natural gas gravity drive and underground gas storage. Petrol. Explor. Dev. 48 (5), 1227–1236. https://doi.org/10.1016/S1876-3804(21)60105-2.
Kowalski, J., Klimkowski, Ł., Nagy, S., 2023. Numerical simulation study on underground gas storage with cushion gas partially replaced with carbon dioxide. Energies 16 (14), 5248. https://doi.org/10.3390/en16145248.
Li, B., Zhu, X., 2019. Grey relational decision making model of three-parameter interval grey number based on AHP and DEA. Grey Syst. Theor. Appl. 10, 25–37. https://doi.org/10.1108/GS-10-2018-0049.
Li, Y., Zhu, S., Guo, S., 2016. Multi-attribute grey target decision method with three-parameter interval grey number. Grey Syst. Theor. Appl. 6 (2), 270–280. https://doi.org/10.1108/GS-05-2016-0010.
Lin, M., Yan, G., Liu, T., Wu, X., Yu, P., 2023. Simulation and optimization of surface gas injection systems for underground gas storage. ACS Omega 8 (35), 32099–32107. https://doi.org/10.1021/acsomega.3c04321.
Liu, G., Dong, X., Jiang, Q., Dong, C., Li, J., 2018. Natural gas consumption of urban households in China and corresponding influencing factors. Energy Policy 122, 17–26. https://doi.org/10.1016/j.enpol.2018.07.016.
Lodi, F., Grasso, G., 2018. Stress-testing the ALFRED design - part III: safety margins evaluation. Prog. Nucl. Energy 106, 433–439. https://doi.org/10.1016/j.pnucene.2018.04.003.
Marbun, B.T.H., Ridwan, R.H., Nugraha, H.S., Sinaga, S.Z., Purbantanu, B.A., 2020. Casing setting depth and design of production well in water-dominated geothermal system with 330 °C reservoir temperature. Energy Rep. 6, 582–593. https://doi.org/10.1016/j.egyr.2020.02.013.

Molíková, A., Vítězová, M., Vítěz, T., Buriánková, I., Huber, H., Dengler, L., Hanišáková, N., Onderka, V., Urbanová, I., 2022. Underground gas storage as a promising natural methane bioreactor and reservoir? J. Energy Storage 47, 103631. https://doi.org/10.1016/j.est.2021.103631.

Mu, L., Liao, X., Yu, Q., Hao, L., Zhang, J., Zhao, J., Wu, J., 2019. Study on Operation Strategy of Aquifer Underground Gas Storage Using CO_2 as Cushion Gas. All Days CMTC-552947-MS. https://doi.org/10.7122/CMTC-552947-MS.

Sadeghi, S., Sedaee, B., 2022. Mechanistic simulation of cushion gas and working gas mixing during underground natural gas storage. J. Energy Storage 46, 103885. https://doi.org/10.1016/j.est.2021.103885.

Saeed, R.A., Recupero, D.R., Remagnino, P., 2020. A boundary node method for path planning of mobile robots. Robot. Autonom. Syst. 123, 103320. https://doi.org/10.1016/j.robot.2019.103320.

Sedaee, B., Mohammadi, M., Esfahanizadeh, L., Fathi, Y., 2019. Comprehensive modeling and developing a software for salt cavern underground gas storage. J. Energy Storage 25, 100876. https://doi.org/10.1016/j.est.2019.100876.

Sheng, Y., Li, W., Lan, K., Jiang, J., Kong, H., 2021. Dynamic design method of wellbore structure during drilling operation based on LWD. J. Pet. Explor. Prod. Technol. 11 (2), 795–804. https://doi.org/10.1007/s13202-020-01048-3.

Tang, L., Wang, J., Ding, G., Sun, S., Zhao, K., Sun, J., Guo, K., Bai, F., 2016. Downhole inflow-performance forecast for underground gas storage based on gas reservoir development data. Petrol. Explor. Dev. 43 (1), 138–142. https://doi.org/10.1016/S1876-3804(16)30016-7.

Vershkov, V.A., Shelukhin, D.A., Subbotin, G.F., Dnestrovskij, YuN., Danilov, A.V., Melnikov, A.V., Eliseev, L.G., Maltsev, S.G., Gorbunov, E.P., Sergeev, D.S., Krylov, S.V., Myalton, T.B., Ryzhakov, D.V., Trukhin, V.M., Chistiakov, V.V., Cherkasov, S.V., 2015. Density fluctuations as an intrinsic mechanism of pressure profile formation. Nucl. Fusion 55 (6), 063014. https://doi.org/10.1088/0029-5515/55/6/063014.

Wei, K., Guan, Z., Wei, J., Fu, S., Zhao, T., 2013. Drilling risk assessment method based on neural network and Monte Carlo simulation. China Saf. Sci. J. 23 (2), 123–128. https://doi.org/10.16265/j.cnki.issn1003-3033.2013.02.016 (in Chinese).

Wei, K., Li, Q., Luan, J., Liu, M., Wang, X., 2020. Formation matrix and its application in drilling risk evaluation. Int. J. Saf. Secur. Eng. 10 (3), 351–357. https://doi.org/10.18280/ijsse.100306.

Wei, K., Wang, C., Wu, D., Guo, Y., Liao, H., 2024. Drilling risk evaluation method based on grey information from adjacent wells. China Saf. Sci. J. 34 (6), 99–108. https://doi.org/10.16265/j.cnki.issn1003-3033.2024.06.1575 (in Chinese).

Xu, Q., Liu, H., Song, Z., Dong, S., Zhang, L., Zhang, X., 2022. Dynamic risk assessment for underground gas storage facilities based on Bayesian network. J. Loss Prev. Process. Ind. 76, 104961. https://doi.org/10.1016/j.jlp.2022.104961.

Xu, Y.Q., Liu, K., He, B.L., Pinyaeva, T., Li, B.S., Wang, Y.C., Nie, J.J., Yang, L., Li, F.X., 2023. Risk pre-assessment method for regional drilling engineering based on deep learning and multi-source data. Pet. Sci. 20 (6), 3654–3672. https://doi.org/10.1016/j.petsci.2023.06.005.

Xue, W., Wang, Y., Chen, Z., Liu, H., 2023. An integrated model with stable numerical methods for fractured underground gas storage. J. Clean. Prod. 393, 136268. https://doi.org/10.1016/j.jclepro.2023.136268.

Yang, M., Zhao, X., Meng, Y., Li, G., Zhang, L., Xu, H., Tang, D., 2017. Determination of transient temperature distribution inside a wellbore considering drill string assembly and casing program. Appl. Therm. Eng. 118, 299–314. https://doi.org/10.1016/j.applthermaleng.2017.02.070.

Yu, W., Gong, J., Song, S., Huang, W., Li, Y., Zhang, J., Hong, B., Zhang, Y., Wen, K., Duan, X., 2019. Gas supply reliability analysis of a natural gas pipeline system considering the effects of underground gas storages. Appl. Energy 252, 113418. https://doi.org/10.1016/j.apenergy.2019.113418.

Zheng, D., Xu, H., Wang, J., Sun, J., Zhao, K., Li, C., Shi, L., Tang, L., 2017. Key evaluation techniques in the process of gas reservoir being converted into underground gas storage. Petrol. Explor. Dev. 44 (5), 840–849. https://doi.org/10.1016/S1876-3804(17)30095-2.

Zhang, B., Cao, J., Lin, S., Li, X., Zhang, Y., Zheng, X., Chen, W., Song, Y., 2024. Optimized inverse distance weighted interpolation algorithm for γ radiation field reconstruction. Nucl. Eng. Technol. 56 (1), 160–166. https://doi.org/10.1016/j.net.2023.09.020.

Zhang, G., Li, B., Zheng, D., Ding, G., Wei, H., Qian, P., Li, C., 2017. Challenges to and proposals for underground gas storage (UGS) business in China. Nat. Gas. Ind. B 4 (3), 231–237. https://doi.org/10.1016/j.ngib.2017.07.025.

Zhang, J., Tan, Y., Zhang, T., Yu, K., Wang, X., Zhao, Q., 2020. Natural gas market and underground gas storage development in China. J. Energy Storage 29, 101338. https://doi.org/10.1016/j.est.2020.101338.

Zhang, L., Du, J., Tian, Z., et al., 2022. Application of seismic-based casing deformation prediction technology in Xinjiang Oil field. Xinjiang Oil & Gas 18 (3), 86–91. https://doi.org/10.12388/j.issn.1673-2677.2022.03.015 (in Chinese).

Zhang, S., Wang, H., Qiu, Z., Cao, W., Huang, H., Chen, Z., 2019. Calculation of safe drilling mud density window for shale formation by considering chemo-poro-mechanical coupling effect. Petrol. Explor. Dev. 46 (6), 1271–1280. https://doi.org/10.1016/S1876-3804(19)60280-6.

Zhu, X., Liu, B., 2020. Three-level assessment for casing in marine gas reservoir. Int. J. Pres. Ves. Pip. 182, 104040. https://doi.org/10.1016/j.ijpvp.2019.104040.